Untersuchung des Effekts amyloidogener Proteine auf intrazelluläre Redox-Haushalte mittels genetisch kodierter Redox-Sensoren

---

Using genetically encoded redox sensors to study the effect of amyloidogenic proteins on intracellular redox environments

Bachelor's Thesis

zur Erlangung des akademischen Grades

Bachelor of Science

Studiengang Biochemie

Fakultät Chemie

Technische Universität München

vorgelegt von

Louise Funke

aus

Fontainebleau, Frankreich

angefertigt in der Arbeitsgruppe

Prof. Dr. Franz-Ulrich Hartl, Max-Planck-Institut für Biochemie

unter Anleitung von

Prof. Michael Groll

München, Juli 2014

Abstract

Proteinaggregate in Form hochstrukturierter amyloider Fibrillen wurden in vielen neurodegenerativen Krankheiten nachgewiesen. Der genaue Mechanismus, wie diese zum Tod neuronaler Zellen führen könnten, ist jedoch noch nicht bekannt. Eine Hypothese ist, dass die Bildung der Aggregate zu einem Ungleichgewicht in der Protein Homöostase führt und dies zu der Entstehung von Stress im endoplasmatischen Retikulum (ER) führt. Da die Redox-Homöostase im ER entscheidend für die Proteinfaltung ist und daher sehr sensitiv auf eine Störung reagiert, kann dauerhafter ER Stress zu der Induktion von oxidativem Stress führen, der sich auf den Redox-Zustand der gesamten Zelle auswirkt. Da oxidativer Stress unter anderem mit der Erhöhung der Konzentration der toxischen reaktiven Sauerstoffspezies H_2O_2 einhergeht, könnte dies ein Auslöser für den beobachteten Zelltod sein.

Diese Hypothese wird durch die Erhöhung verschiedener Marker für ER Stress und oxidativen Stress in Zellen von Patienten mit neurodegenerativen Erkrankungen gestützt. Um diese These zu untersuchen, haben wir künstliche β-Proteine, die amyloide Fibrillen bilden und daher die Aggregate von neurodegenerativen Krankheitsproteinen simulieren, sowohl im Cytosol als auch im ER der menschlichen Zelllinie HEK293 exprimiert. Deren Effekt auf den Redox-Zustand wurde mit zwei verschiedenen Redox-Sensoren, roGFP und HyPer, *in vivo* in Duchflusszytometrie-Experimenten untersucht. Nach der erfolgreichen Etablierung der Methoden zur Messung der Sensoren, konnten wir einen deutlichen reduzierenden Effekt der β-Proteine sowohl im Cytosol als auch im ER detektieren. Dies entspricht interessanterweise dem gegenteiligen Effekt, der nach der Auslösung von oxidativem Stress erwartet worden wäre.

Table of Contents

Abbreviations:

- AD: Alzheimer's disease
- APP: Amyloid precursor protein
- BCA assay: Bicinchoninic acid assay
- BSA: Bovine serum albumin
- DMEM: Dulbecco's Modified Eagle Medium
- DTT: Dithiothreitol
- EGFP: Enhanced GFP
- ERO-1: Endoplasmic reticulum oxidoreductin-1
- FACS: Fluorescence activated cell sorting
- FBS: Fetal Bovine Serum
- FITC: Fluorescein Isothiocyanate
- FSC-H: Forward scatter height
- GSH: Glutathione
- GSSG: Glutathione disulphide
- HRP: Horseradish peroxidase
- HEK293 cells: Human Embryonic Kidney 293 cells
- MOPS buffer: 3-(N-morpholino)propanesulfonic acid buffer
- NEAA: Non-essential amino acids
- NFTs: Neurofibrillary tangles
- PBS: Phosphate Buffered Saline
- PD: Parkinson's disease
- PDI: Protein Disulphide Isomerase
- PN: Proteostasis Network
- RIPA buffer: Radioimmunoprecipitation assay buffer
- roGFP: Redox sensitive GFP
- ROS: Reactive oxygen species
- SSC-A: Side scatter area
- TBS: Tris-buffered saline
- TBST: Tris-buffered saline with 0.1 % Tween 20
- UPR: Unfolded Protein Response
- wt-GFP: Wild type GFP

I. Introduction

1. Protein aggregation and neurodegenerative diseases

With the aging population neurodegenerative diseases have emerged as one of the main future challenges for society and as a result have moved into the focus of biomedical research. Despite the extensive research, which has revealed many deviations connected to the diseases on a cellular level, the causality and mechanism are still not understood. Hence, currently available treatments at best only address the symptoms rather than the cause of the diseases.

A hallmark of neurodegenerative diseases is the aggregation and deposition of abnormal proteins involved in the progressive loss of function and structure, and finally the death of neurons (Taylor et al., 2002). Here the toxicity of the proteins seems to strongly correlate with their capacity to aggregate (Rubinsztein, 2006). The propensity for a protein to form aggregates mainly depends on the chemical properties of its amino acid sequence, its conformational stability and concentration in the cell (Chiti and Dobson, 2006; Ciryam et al., 2013). A driving factor of protein folding are hydrophobic forces between hydrophobic patches that are normally buried inside the protein. If these hydrophobic patches are exposed they provide surfaces for aberrant protein interactions and thus are also a main driving factor behind aggregation. Protein aggregation can either occur in the form of amorphous structures or as highly ordered fibrillar structures, the so-called amyloids (Hartl and Hayer-Hartl, 2009; Kim et al., 2013). The latter are characterised by β strands running perpendicular to the fibril axis (cross-β structure) and are associated with many neurodegenerative diseases (Hartl and Hayer-Hartl, 2009; Kim et al., 2013).

Cells contain a substantial fraction of metastable proteins that are intrinsically unstructured in order to achieve the flexibility to interact with a variety of binding partners. To prevent these proteins from aggregation cells have developed an extensive network to maintain protein homeostasis (proteostasis) including molecular chaperones and degradation machineries (Hartl et al., 2011; Hipp et al., 2014). When the capacity of the proteostasis network (PN) is exceeded, misfolding and aggregation of endogenous proteins can not be completely prevented anymore and these additional misfolded proteins further occupy and sequester the PN leading to a vicious cycle that eventually results in proteostasis collapse and cell death (Hipp et al., 2014). Neurodegenerative disease proteins are particularly harmful to the cellular proteostasis because their aggregates were found to directly impair components of the PN (Olzscha et al., 2011; Park et al., 2013). One of the main risk factors that initialises the aggregation of neurodegenerative disease proteins is aging, as it leads to a decline in the PN capacity (David et al., 2010; Morimoto, 2008) and hence may trigger the vicious cycle described above.

In spite of the common pattern of neurodegenerative diseases, the responsible proteins as well as the location of their aggregates are

characteristic for the particular disease (Rubinsztein, 2006; Taylor et al., 2002). For example, in Parkinson's disease (PD) aggregates, called Lewy bodies, are predominantly cytosolic with the main disease protein being α-synuclein, whereas in Alzheimer's disease (AD) the aggregates are found as both extracellular plaques (Aβ peptide) and intracellular tangles (tau protein). Still, it is suspected that the underlying principle of toxicity is very similar for these proteins, because of several commonalities that were found. Firstly, many disease proteins (e.g. α-synuclein, Aβ, proteins with polyglutamine repeats) form amyloid fibrils, higher order structures that involve β strands and β turns, which build up fibrous aggregates (Ross and Poirier, 2004). Secondly, soluble profibirillar intermediates preceding aggregation have been widely observed in several neurodegenerative diseases and different studies suggest that these intermediates strongly contribute to toxicity (Campioni et al., 2010; Ross and Poirier, 2004; Sánchez et al., 2003; Walsh et al., 2002). Finally, most of the disease proteins show a gain-of-function toxicity in the form of new toxic functionality (Ross and Poirier, 2004; Rubinsztein, 2006). In conclusion, a common mechanism behind the neurodegenerative diseases is highly suspected and therefore understanding the principle and developing a therapy for one of them may be applicable to the others.

Neuronal cells in disease specific regions of the nervous system are mainly affected because they are particularly vulnerable to toxic effects of abnormal proteins (Saxena and Caroni, 2011), and since they normally cannot reproduce they are not replaced when they die (Nowakowski, 2006). This results in the well-known symptoms of neurodegenerative diseases such as motoric deterioration in PD or the decline in mental ability impairing memory, thinking and judgment in the case of AD.

2. Artificial amyloidogenic proteins

The underlying cellular mechanisms of aggregate toxicity are not yet fully understood. A promising attempt to investigate the aggregate toxicity is the use of artificial β sheet proteins (β proteins) as models for amyloid-like aggregation. β proteins were designed as an alternating pattern of polar and nonpolar residues, which determines the β strand secondary structure (Xiong et al., 1995), with the specific side chains varied combinatorially (West et al., 1999). β proteins spontaneously aggregate into amyloid-like cross-β fibrils, emulating the aggregation properties of disease proteins such as Aβ peptides, prion proteins and α synuclein (Olzscha et al., 2011). Importantly, β proteins cause significant toxicity when expressed in human cells (Olzscha et al., 2011). The main advantage of these artificial proteins is that they have no physiological function and therefore allow the explicit study of a gain-of-function toxicity without interference of possible effects from excessive or loss of physiological function.

The specific protein from the combinatorial library (West et al., 1999) investigated in this thesis is β23. The protein is made up of six β strands each consisting of seven amino acids in a polar-nonpolar alternating pattern, connected by 4-amino acid linker segments and with a c-Myc-tag attached to the N-terminus (Figure 1). β23 was found to have a high β sheet propensity because of its large isoleucine content resulting in strong β aggregation

(Olzscha et al., 2011; Tartaglia et al., 2008). Further, the presence of profibirillar species was detected under physiological conditions and toxicity of the protein was demonstrated through a significant reduction of cell viability upon expression in HEK293T cells for 3 days (Olzscha et al., 2011).

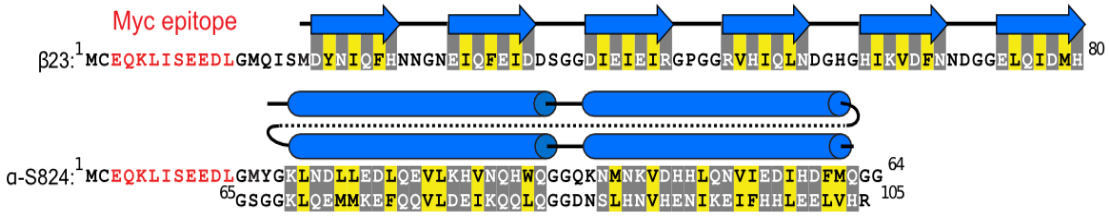

Figure 1: Primary and secondary structure of the artificial amyloidogenic protein β23 and the soluble control protein α-S824. Polar and nonpolar amino acids are marked in grey and yellow respectively, β strands and α helices by blue arrows and rods. This figure was adapted from Olzscha et al., 2011.

As a control the designed α helical protein α-S824 of similar amino acid composition as the model protein β23 but with a 4-Helix bundle secondary structure (hence termed α protein) was used (Figure 1) (Wei et al., 2003). This protein did not reduce cell viability and could also be recovered completely in the soluble fraction after cell fractionation, while the β protein was mainly found in the insoluble fraction (Olzscha et al., 2011). Many neurodegenerative proteins such as the Aβ peptide are processed in the secretory pathway (Cook et al., 1997; Wild-Bode et al., 1997). We thus decided to also examine the behaviour of artificial β proteins that are targeted to the ER for secretion. For this purpose, we used an ER-targeted version of β23 (sp-β23), where the ER-targeting signal peptide of the human lung surfactant protein B (Sp-B) is fused to the N-terminus of the protein.

3. Alzheimer's disease

With more than 35 million affected people worldwide and being the main cause of dementia (over 50 % of cases) AD is the most common and therefore best-studied neurodegenerative disease (Querfurth and LaFerla, 2010) and will serve as an exemplary neurodegenerative disease in this thesis. The disease can be hereditary and sporadic with age being the principal risk factor (Lindsay et al., 2002). The macroscopic manifestation of AD emerges as the up-regulation of microglial inflammatory response (Wyss-Coray, 2006) and a synaptic degradation (Selkoe, 2002) resulting in a diffuse atrophy of the Cortex and the Hippocampus. On a cellular level, the two characteristics of AD are neuritic plaques and neurofibrillary tangles.

Neuritic plaques are extracellular aggregates largely made up of β amyloid (Aβ) peptides. These naturally result from proteolytic cleavage of the amyloid precursor protein (APP) generating a variety of Aβ species ranging from 39 to 42 ($Aβ_{39}$ – $Aβ_{42}$) amino acids in length (Madeo, 2013; Querfurth and LaFerla, 2010). The $Aβ_{42}$ monomer is especially prone to form amyloid deposits, whereas the much more prevalent shorter $Aβ_{40}$ peptide is much less amyloidogenic (Dahlgren et al., 2002). The Aβ monomers can spontaneously self-aggregate into various forms, but soluble oligomers and aggregate

intermediates seem to be the most toxic (Dahlgren et al., 2002; Walsh and Selkoe, 2007).

The second characteristic, neurofibrillary tangles (NFTs) are intracellular filamentous lesions which mainly consist of an abnormally hyperphosphorylated form of the protein tau, a cytoskeletal protein abundant in neurons (Querfurth and LaFerla, 2010). NTFs are also found in other neurodegenerative diseases termed tauopathies presenting another commonality (Lee et al., 2001). Experimental results however suggest that tau aggregation occurs after Aβ accumulation (Götz et al., 2001).

4. Current status of research in AD

In the last decade, an immense amount of studies on AD have uncovered many distinctive features (Querfurth and LaFerla, 2010). Besides mutations, which may alter the protein's structure to be more prone to aggregation, aggregation prone disease proteins often show additional covalent modifications such as phosphorylation in the case of hyperphosphorylated tau or α-synuclein and oxidative modifications (Ross and Poirier, 2004). With regard to the immediate effects of amyloid aggregates, several studies suggest that the misfolding proteins interfere with the chaperone machinery of the cell thus impairing the protein quality control and clearance mechanisms and resulting in a dysfunction of proteostasis (Bence et al., 2001; Gidalevitz et al., 2006). Furthermore, experiments with model membranes showed a disruptive effect of oligomeric intermediates on the integrity of lipid membranes (Lashuel and Lansbury, 2006). Finally, using quantitative proteomics, it was demonstrated, using artificial β proteins, that the resulting aggregates interact with a wide range of other cellular proteins (Olzscha et al., 2011) leading to their sequestration, malfunction and probably the loss of essential cellular functions (Olzscha et al., 2011).

The examination of AD brain cells compared to age-matched controls revealed a characteristic increase in the concentrations of zinc, copper and iron ions (Lovell et al., 1998) as well as severely deformed and defective mitochondria (Rui et al., 2006). Additionally, high levels of oxidised proteins, advanced glycation end products and lipid peroxidation and oxidative modifications in nuclear and mitochondrial DNA, indicated by accumulation of the oxidative marker 8OHG (Madeo, 2013; Mecocci et al., 1994) strongly point to the occurrence of oxidative stress in the AD brain. Furthermore, advanced ER stress could be detected due to significantly elevated levels of several ER stress markers (Hoozemans et al., 2009; Unterberger et al., 2006). All of these characteristics can be linked by oxidative stress, which is also enhanced in aging cells. The mechanisms behind oxidative stress are extremely diverse and intertwined, so until now causalities and processes behind the events observed in AD brain cells are still unclear. Below, the background and the hypothesised connections will be explained as well as the potential role of Aβ in this context.

Oxidative stress is characterised by an imbalance between the cellular production of or exposure to reactive oxygen species (ROS) and the cell's antioxidant machinery that protects cellular homeostasis from oxidative

disruption through ROS (Yu, 1994). ROS are a natural by-product of normal metabolism of oxygen, in particular of the respiratory chain. In excess they can cause molecular damage in proteins, lipids and DNA, leading to critical failure of biological function (Gella and Durany, 2009; Yu, 1994). Another important source of ROS is the ER, where oxygen acts as the final electron acceptor in the course of oxidative protein folding (Figure 2). Most proteins that pass through the ER contain disulphide bridges to stabilize them in their final extracellular destination. The formation of disulphide bonds is driven by the protein disulphide isomerase (PDI), which is reduced while oxidising thiol groups of substrate proteins and in turn is re-oxidised through endoplasmic reticulum oxidoreductin-1 (ERO-1). ERO-1 then transfers electrons to molecular oxygen for regeneration resulting in the formation of the ROS H_2O_2. To reverse non-native disulphide bonds glutathione (GSH), the main cellular redox buffer, assists in reducing them again and is itself oxidised to glutathione disulphide (GSSG). The GSH/GSSG ratio also determines the highly oxidising environment in the ER, which is necessary for protein folding and disulphide formation. The ratio is thus extremely low (between 1:1 and 3:1) in the ER lumen compared to the cytoplasm (>50:1) (Hwang et al., 1992). Therefore, when accumulation of misfolded proteins occurs, a state referred to as ER stress, the refolding enzymes are depleted after activation of the unfolded protein response (UPR), which leads to the upregulation of several proteostasis factors to counteract aggregation. However, in the regeneration process increased amounts of the by-product H_2O_2 are formed. This is one way how oxidative stress is induced by ER stress.

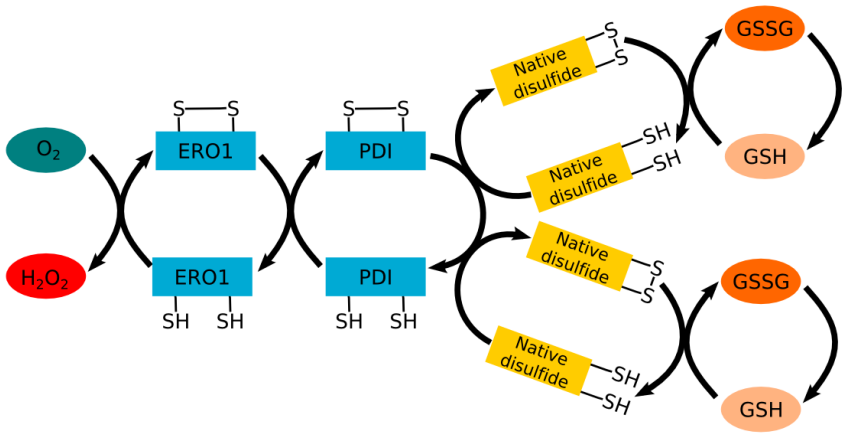

Figure 2: Schematic overview of the processes during oxidative protein folding in the ER. These lead to the formation of the reactive oxygen species H_2O_2 and influence the ratio of the redox pair GSH/GSSG. Figure adapted from Bhandary et al., 2012.

Alternatively, oxidative stress can be induced as a result of alterations in the Ca^{2+}-environment of the ER lumen, which is the major site of calcium storage. Upon ER stress Ca^{2+} is released into the cytosol and from there is taken up by the mitochondria and the nucleus (Murphy, 2009). In the mitochondria this leads to an alteration of the membrane potential and stimulation of mitochondrial metabolism, which subsequently increases ROS production. In parallel, the respiratory chain is further stimulated by ER stress through the associated increased ATP consumption from chaperone activity (Bhandary et

al., 2012). The ER and mitochondria are in close proximity in the cell and maintain direct physical connections allowing for a fast and efficient crosstalk between the two compartments (Patergnani et al., 2011; Rizzuto et al., 1998). Furthermore, ROS themselves have a stimulating effect on Ca^{2+} channels, enhancing the Ca^{2+} release from the ER even more. As the antioxidant potential of the cell diminishes this vicious cycle continues, finally leading to apoptosis (Malhotra and Kaufman, 2007; Walter and Ron, 2011). Since synapses are sites of especially high energy demand and require exact Ca^{2+} regulation, this explains why they are so sensitive to oxidative stress and hence strongly impaired in neurodegenerative diseases (Du et al., 2010; Ferreiro et al., 2012). In summary, prolonged ER stress can lead to oxidative stress by initiating ROS production in the ER and/or the mitochondria.

In this complex network, several direct effects of Aβ have been observed, thus proving the relevance of oxidative stress to AD and probably other neurodegenerative diseases. Firstly, in AD tissues Aβ was found to bind copper forming Aβ:Cu complexes (Hou and Zagorski, 2006). These complexes were observed to generate neurotoxic H_2O_2 from oxygen through Cu^{2+} reduction, thus constituting Aβ as an oxidant. On the one hand, as mentioned above, several metal ions, including copper, are highly enriched in AD cells and it is hypothesised that H_2O_2 production by the complex as well as exhaustion of reducing agents may contribute to the neurotoxicity of Aβ in AD (Huang et al., 1999; Opazo et al., 2002). On the other hand, several studies on the contrary observed an antioxidant effect of Aβ. However, this antioxidant effect may actually be triggered as a response to prior oxidative stress (Baruch-Suchodolsky and Fischer, 2009; Sinha et al., 2013). This issue is highly debated (Atwood et al., 2003) and subject of current research. Secondly, Aβ was shown to induce Ca^{2+} release from the ER (Ferreiro et al., 2004, 2006). Thirdly, Aβ could be localised to mitochondrial membranes and was found to be responsible for ROS generation and mitochondrial dysfunction in the energy metabolism. These effects were visible long before cell death, identifying it as an early event in AD (Reddy et al., 2010). These findings, together with the observation of ER stress and oxidative stress markers in AD brains, strongly indicate that Aβ induces oxidative stress resulting in a vicious circle finally leading to apoptosis. Nevertheless, how exactly Aβ induces oxidative stress is presently unclear. To explore this in greater detail, measurements of intracellular and even compartment specific *in vivo* redox state offer a promising way forward.

5. Redox sensing

When measuring the cellular redox state it has to be defined which compartment and which redox couple from the multitude of cellular redox pairs such as $NADPH/NADP^+$, GSH/GSSG, O_2/H_2O_2 should be detected. These redox pairs differ in their kinetics and thermodynamics and are far from equilibrium with each other (Meyer and Dick, 2010). Some conventional methods for detection of redox states include enzymatic assays and HPLC or gel mobility, but these all share the same limitations of specificity due to oxidation artefacts caused by cell disruption, irreversibility and lack of compartment specificity (Meyer and Dick, 2010). A promising solution to overcome these limitations is a newly developed class of genetically encoded

in vivo redox sensors designed to specifically detect a certain redox pair. These sensors are based on fluorescent proteins that were modified in such a way that their fluorescence depends on their redox state. This method provides an elegant and very easy way to perform specifically localised *in vivo* measurements of the cellular redox state and has the additional advantage of being reversible allowing even kinetic analysis. Furthermore, the fluorescent proteins can be directed to specific compartments by insertion of signal sequences.

5.1. roGFP

One of these new sensors is redox-sensitive GFP (roGFP). We used roGFP1, which is a mutant of enhanced GFP (EGFP). EGFP is a variant of wild-type GFP (wt-GFP) from the jellyfish *Aequorea victoria* showing the same emission spectrum but due to a few chromophore mutations it is 35 times brighter than wt-GFP and codon-optimised for expression in higher mammalian cells making it a much more sensitive reporter protein (Zhang et al., 1996). roGFP was developed by introducing four mutations into EGFP (C48S, S65T, S147C, Q204C); thus, generating a new disulphide bridge (Hanson et al., 2004). Structurally this 238 amino acid long polypeptide still shows the 11-stranded β barrel with an internal α helix characteristic of wt-GFP (Figure 3).

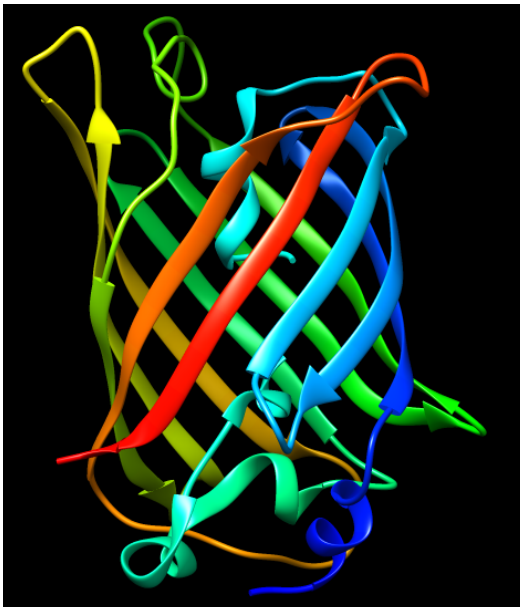

Figure 3: Crystal structure of roGFP in its reduced form. roGFP shows the characteristic β barrel structure of GFP. The structure was derived from the PDB entry 1JC0,

The introduction of two cysteines at positions 147 and 204, which are located on the adjacent β strands 7 and 10 close to the GFP chromophore, leads to the reversible formation of a disulphide bond in an oxidising environment. Upon formation of the disulphide bond the β strands are shifted causing several small structural rearrangements and leading to a ratiometric shift in the excitation spectrum of roGFP. The significant movements are shown in sections from the reduced and oxidised crystal structures – PDB entries 1JC0 and 1JC1 respectively – (Figure 4) (Meyer and Dick, 2010). It has been suggested that these changes influence the protonation state of the

chromophore since an increase in the chromophore's protonation state was seen upon oxidation, which may explain the shift in fluorescence (Hanson et al., 2004).

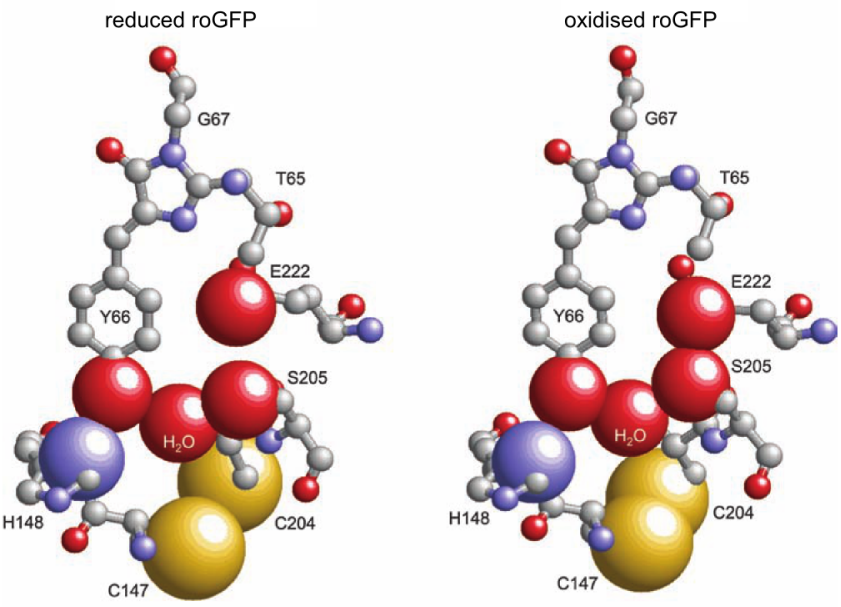

Figure 4: Conformational changes of the roGFP chromophore upon change in the redox state. The figure shows the relevant part of the redox sensor in its reduced (left) and oxidised (right) form, where important atoms are shown as Van-der-Waals spheres (yellow: sulphur, red: oxygen, purple: nitrogen). Formation of the disulphide bond C147-C204 leads to a shift of the residues H148 and S205 relative to the chromophore influencing the proton transfer between the chromophore and E222. The resulting change in the protonation state of the chromophore is suggested to be the cause of the fluorescence shift. Figure adapted from Meyer and Dick, 2010.

The ratiometric shift refers to the inverse behaviour of the fluorescence intensities of the two excitation maxima at ~400 nm and ~490 nm. This allows a ratiometric analysis of the measured redox state by calculating the ratio between the maximal intensities, usually measured at 405 nm and 488 nm. This ratio calculation makes the measurement independent of protein concentration and thus reduces data distortion through photo bleaching or non-uniform indicator distribution (Hanson et al., 2004). Even pH effects on the fluorescent protein can be cancelled out for pH values between 5.5 and 8.0 by ratio calculation, because both excitation wavelengths are affected equally (Meyer and Dick, 2010; Schwarzländer et al., 2008). A high ratio $I_{405\ nm}/I_{488\ nm}$ indicates a large fraction of oxidised roGFP, i.e. an oxidising environment, while a low ratio corresponds to mainly reduced roGFP. The maximal dynamic range of the ratio can be determined by full oxidation and reduction of the sensor by applying redox agents such as H_2O_2 for oxidation and DTT for reduction. roGFP was shown to predominantly respond to the glutathione redox pair GSH/GSSG (Meyer et al., 2007), which should be kept in mind when interpreting experimental results because the redox couple cannot be considered representative of all redox processes that occur in a cell

at a certain time. This means that when H_2O_2 and DTT are used as redox agents, roGFP only indirectly senses these substances through a change in the GSH/GSSG ratio as a reaction of the cell. Based on this finding an even more sensitive version of roGFP directly coupled to glutaredoxin, a redox enzyme using glutathione as a cofactor hence acting as a mediator between glutathione and roGFP, (Grx-roGFP) was designed (Gutscher et al., 2008), but was not used in the experiments presented below.

5.2. HyPer

Another redox sensor, HyPer, was designed to specifically detect intracellular H_2O_2 concentrations (Belousov et al., 2006). To this end, cpYFP, a circularly permuted yellow fluorescent protein where the original amino and carboxy termini are fused by a polypeptide linker and new termini are introduced close to the chromophore, was inserted into the regulatory domain of the prokaryotic H_2O_2-sensing protein OxyR. The naturally redox active domain of OxyR contains an active cysteine residue C199 which reacts with H_2O_2 to form a cysteine sulfenic acid (S-OH) which then forms an intramolecular disulphide bridge with a second cysteine C208 in the same domain leading to a conformational change. CpYFP, was integrated into this changing region (between residues 205 and 206) and the resulting cpYFP-OxyR chimera, HyPer, hence displays an H_2O_2 dependent change in the fluorescence. As with roGFP, the two excitation maxima at 420 nm and 500 nm (Belousov et al., 2006) show inverse behaviour and allow a ratiometric analysis. The chromophore also changes its protonation state and the reaction was shown to be reversible (Belousov et al., 2006). To facilitate experimental analysis the standard wavelengths 405 nm and 488 nm can be used and for better comparability to roGFP the ratio $I_{488\ nm}/I_{405\ nm}$ was calculated for Hyper. Thus, both sensors give high ratios for oxidative conditions and low ratios for reducing ones. In contrast to roGFP, HyPer shows certain pH dependence reflected in these ratios (Belousov et al., 2006), but since the pH in cells is usually kept constant this should not influence intracellular measurements. The high specificity of HyPer for H_2O_2 is thought to account for HyPer localised to the cytosol and the nucleus, which harbour potent disulphide-reducing machineries, but it is debated whether this sensitivity also persists in the ER where oxidising factors such as PDI may also interact with HyPer (Birk et al., 2013). Besides specificity, HyPer also shows extreme sensitivity for H_2O_2, sensing low micromolar concentrations in the cell making the sensor about 25 times more sensitive than roGFP (Malinouski et al., 2011).

6. Research aims

The aim of the presented research is to use these powerful new redox sensors to investigate the effect of β proteins on the cellular redox state. By selectively measuring two of the main cellular redox systems (the GSH/GSSG redox pair and H_2O_2/O_2) the co-expression of the sensors and artificial β proteins in human cell lines may reveal effects of β proteins on the cellular redox state. Studying the effects of β proteins may reveal some common mechanisms of aggregate toxicity that will allow a better understanding of the underlying cellular mechanisms causing neurodegeneration. Since the ER was found to play a crucial role in the context of AD and oxidative stress, the

sensors as well as the β proteins will also be directed to the ER via specific targeting signal peptides to measure the local effects there in addition to cytosolic effects. First, the sensors were established in the two cellular compartments and then a suitable experimental setup was developed to measure the effects of β23 and sp-β23 expressed in HEK293 cells using FACS and microscopy. With a better understanding of the precise relation between the disease proteins and oxidative stress new therapeutic strategies may be developed in the future.

II. Materials and Methods

1. Cell culture

Maintenance

HEK293 cells were cultured in DMEM medium (Biochrom) supplemented with 10 % Fetal Bovine Serum (FBS), L-glutamate, Pen/Strep (100 U/ml penicillin and 100 µg/ml streptomycin) and non-essential amino acids (NEAA). Cells were maintained in 10 cm plates in 10 ml medium in a 37 °C incubator with 5 % CO_2 and 85-95 % humidity. Solutions used for cells cultures were always pre-warmed for at least 10 min in a 37 °C water bath.

Thawing

A 1 ml aliquot of cells was thawed by briefly holing it into a 37 °C water bath and then adding a small amount of warm growth medium to the frozen cells to speed-up thawing. Thawed cells were transferred to a falcon tube containing 10 ml growth medium to rapidly dilute the freezing medium. This step was repeated until the whole suspension was thawed and transferred. Then the cell suspension was pelleted by centrifugation and after discarding the supernatant, the cell pellet was resuspended in 10 ml fresh growth medium and transferred to a 10 cm plate.

Splitting

The medium was removed and cells were washed with 5 ml PBS, carefully pipetting against the wall of the plate. To detach them, cells were incubated with 1 ml TrypLE (Gibco) for approximately 5 min. After confirming full detachment using a microscope another 9 ml of fresh medium were added and the solution was pipetted up and down several times to completely resuspend all cells. Then the amount of the suspension needed for the requested dilution was taken and added to a new plate prepared with fresh medium. The cells were split 1:6 for a two day culture or 1:10 to last three days.

Seeding

Cells were trypsinised as described. From the 10 ml cell suspension an aliquot of 100 µl was diluted in 900 µl PBS and counted with a Millipore Handheld Automated Cell Counter with 60 µm tips. The Counter was adjusted to only select cells with a diameter of around 18 µm. To ensure a reading within the linear range, the count was only accepted in the range of 10^4-10^6 cells and otherwise repeated with a higher dilution. Then the amount of cells needed was calculated and the corresponding volume was taken from the cell suspension onto a new plate and diluted with the appropriate amount of medium. Cells were either seeded in 10 cm plates in 10 ml solution, 6-well plates in 2 ml solution or 12-well plates in 1 ml solution.

2. Plasmid DNA

The plasmids of the four redox sensors (ER-roGFP, cyto-roGFP, ER-HyPer, cyto-HyPer) were kindly provided to us by the group of Kaz Nagata, Kyoto

Sangyo University, Japan. The signal sequence of the ER-targeted β23 was inserted by the group of Jan Johannson, Karolinska Institute, Stockholm, Sweden.

3. Transfection

The transfection reagent FuGENE6 (Promega) was diluted at 3:100 in the reduced serum medium OptiMEM (Life Technologies) (15 µl FuGENE6 for transfection of a 10 cm plate or 3 µl for transfection of one well from a 6-well plate) and incubated for exactly 5 min at room temperature (RT). After adding the plasmid DNA the solution was incubated for another 15 min at RT. A ratio of 1:3 of DNA (µg) to FuGENE (µl) was used for transfection of HEK293 cells. The ratio refers to the total amount of DNA for transfection. For a single transfection 5 µg of plasmid DNA was used and for cotransfection with two plasmids 2.5 µg of each plasmid was used. After incubation the solution was distributed equally onto the cells. Due to the low toxicity of the transfection reagent no media changes were required.

4. Western Blotting

Cells were treated with the redox agents DTT (20 mM) and H_2O_2 (50 mM) 48 h after transfection and incubated for 5 min before the medium was aspirated and the cells were harvested in cold PBS. After centrifugation (4 °C, 5 min, 5000 x g) the pellet was resuspended in lysis buffer (RIPA buffer (Invitrogen) supplemented with a protease inhibitor cocktail (Roche) and benzonase (0.1 U/µl)). The lysate was split into two fractions and DTT (1 mM) was added to one fraction (fraction 1), but not to the other (fraction 2). Both fractions were incubated on ice and vortexed repeatedly for 30 min. Cell lysates were centrifuged (4 °C, 5 min, 5000 xg) to clear cell debris and transferred to fresh tubes. Protein concentrations were measured using a BCA assay (Pierce). Reduced lysates (fraction 1) were denatured in reducing sample buffer (4 M Urea, 2.5 % SDS, 100 mM Tris (pH 6.8), 0.1 mM EDTA, 0.05 % Bromophenolblue, 10 % glycerol, 5 % beta-mercaptoethanol) and non-reduced lysates (fraction 2) in non-reducing sample buffer (without beta-mercaptoethanol). All fractions were incubated at 70 °C for 10 min to ensure complete protein denaturation. The fractions were run on two separate Bis-Tris gels (8 % stacking gel, 12 % separating gel) in separate chambers with MOPS running buffer. For the reducing gel an additional antioxidant (5 mM sodium bisulfate) was added to the running buffer. For each gel the proteins were transferred onto a nitrocellulose membrane in a wet transfer procedure and a ponceau stain of the membrane was performed to confirm the successful transfer. The membranes were blocked with 5 % milk in TBST for 1 h at RT before the primary antibody (anti-GFP mouse monoclonal antibody, 1/1000 in 5 % milk in TBST, Roche) was added for incubation at 4 °C over night. The membranes were washed three times for 10 min with TBST. Then the secondary antibody (goat anti-mouse IgG HRP conjugated, 1/5000 in TBST, Sigma) was added for 1.5 h at RT. After another washing step (3x, 10 min, TBST) the membranes were incubated in TBS for 5 min before they were developed with the Luminata Classico Western HRP substrate (EMD Millipore). After washing in TBST, the membranes were incubated with anti-

GAPDH mouse monoclonal antibody (Millipore) for 1 h at RT followed by washing steps as before and incubation in anti-mouse IgG HRP conjugated (1/5000 in TBST, Sigma) for 1.5 h at RT, washing and developing as before.

5. Microscopy

For microscopy cells were seeded onto poly-lysine covered coverslips (BD Bio-Coat) in a 12-well-plate. Fixing and staining of the cells was performed 48 h post transfection under non-sterile conditions. During incubation times the plate was always kept on a slowly rocking orbital shaker and covered with tin foil to protect the chromophores from light. The media was aspirated. The coverslips were then washed twice for 5 min with 1 ml PBS. Subsequently, the cells were fixed with 500 µl 4 % paraformaldehyde for 1 h at RT. After two additional washing steps (5 min, 1 ml PBS) 0.1 % Triton-X-100 was added to permeabilise the cells for exactly 5 min. The washing steps were repeated (2x, 5 min, 1 ml PBS) and then the coverslips were incubated with 500 µl of 1 % BSA (Serva Fraktion V) sterile filtered in PBS for 1 h at RT to block non-specific antibody binding. Then the cells were incubated for at least 1 h at RT with the primary antibody diluted in 1 % BSA in PBS solution. The coverslips were washed again (3x, 5 min, 1 ml PBS) and then incubated in secondary antibody for 1 h at RT. Two final washing steps were applied before the coverslips were carefully taken from the well and placed upside down on a drop of fluorescent mounting medium onto a microscope glass slide. The mounted slides were left on the bench to dry for a few hours before short-term storage at 4 °C until analysis. The primary antibodies used in the experiments were mouse monoclonal anti-Myc antibody (SC-40 (9E10), Santa Cruz Biotechnology) and rabbit polyclonal anti-ERp57 antibody (Abcam) each at a dilution of 1/500. The secondary antibodies used were: Cy3 labelled goat anti-mouse IgG (Jackson ImmunoResearch), Cy3 labelled anti-rabbit IgG (Dianova) and Alexa Fluor 488 labelled anti-rabbit IgG (Invitrogen), each in a 1/200 dilution.

Samples were analysed by confocal microscopy using a LSM780 microscope (Zeiss) with a 63x objective. Single slice images were recorded using the Zen 2011 software. Cells were excited with 405 nm, 488 nm and 514 nm argon lasers and fluorescence emission was detected with the band pass filters Cy3 (for Cy3 conjugated antibodies), Alexa Fluor 488 (for Alexa Fluor 488 labelled antibodies), EGFP (for wt-GFP and the redox sensors) and AmCyan1 (for detection of the redox sensors).

6. Plate reader

To record the excitation spectra of the redox sensors cells were trypsinised 48 h after transfection and resuspended in PBS. After centrifugation at 200 x g for 3 min the cell pellet was washed with 1 ml HEPES buffer (20 mM HEPES, 130 mM NaCl, 5 mM KCl, 1 mM $CaCl_2$, 1 mM $MgCl_2$, 5.5 mM Glucose, pH 7.4) and spun down again for 3 min at 200 x g. Then the cells were resuspended in HEPES buffer and distributed in a 96-well plate (100 µl per well). The plate was spun down 2 min at 200 x g to generate a cell monolayer at the bottom. Cells were treated by addition of 100 µl of HEPES buffer containing either DTT or H_2O_2 at different concentrations and incubated at

room temperature for indicated times. 100 µl HEPES buffer was added to untreated control samples. An Infinite M1000 Pro plate reader (Tecan) was used for analysis with the excitation spectrum set from 350 to 500 nm for roGFP and from 390 to 520 nm for HyPer with 5 nm intervals each. Emission was detected at 530 nm.

7. Flow cytometry

FACS analysis was performed with a FACSAria III (BD Biosciences) flow cytometer with approximately 50,000 cells per condition. The data was analysed with the FlowJo software. Before FACS analysis cells were harvested by trypsinization and resuspended in PBS. After centrifugation for 5 min at 1300 rpm the pellet was resuspended in an appropriate volume of FACS buffer (PBS with 2 % FBS). Approximately 300 µl of cell suspension were needed per measurement. To analyse the redox sensors the AmCyan filter (510/50) was applied for excitation with the 405 nm laser and the FITC filter (530/30) for the 488 nm laser. During setup the voltage of the channels were adjusted so that the peaks for untransfected cells were set to approximately the same minimum intensity in both channels.

Experimental setup

The experimental setup for a FACS analysis of sensor-transfected HEK cells was established in the following way:

- Day 1: Seeding cells at a density of 5 x 10^4 cells/ml (i.e. 5 x 10^5 cells onto a 10 cm plate, 1 x 10^5 cells in a well of a 6-well-plate). If only one sample was to be analysed from a transfection a 6-well-plate was enough, but for more samples a 10 cm plate was prepared.
- Day 2: Transfection (approximately 24 h after seeding).
- Day 3: Splitting cells 1:2, potentially keeping both fractions for more cells.
- Day 4: Harvesting of cells and FACS analysis.

III. Results and Discussion

1. Establishing the redox sensors

To establish the redox sensors roGFP and HyPer as localised *in vivo* reporters of the cellular redox environment, we recorded their excitation spectra and confirmed their localisations and their ratiometric properties, which should make them independent of the sensor concentration. We further used redox agents to fully oxidise and reduce the sensors in order to determine their dynamic range, while excluding falsifying effects of the redox agents on the autofluorescence of the cells.

1.1. Excitation spectra of the redox sensors

The redox sensors roGFP and HyPer were used in two forms, one ER-targeted version and one version without a signal peptide (henceforth called cytosolic version). To confirm that the published excitation spectra (Belousov et al., 2006; Hanson et al., 2004) also apply to our versions of the sensors, all four spectra were recorded with a plate reader after expression of the sensors in HEK293 cells. To achieve maximal reduction and oxidation the sensor transfected cells were treated with the redox agents DTT and H_2O_2 respectively.

The roGFP spectrum (Figure 5) is characterised by two excitation maxima at approximately 400 nm and 480 nm. Upon oxidation (red curve) the chromophore should gain excitability in the blue range and loose excitability in the higher nm range, whereas reduction (green curve) should have the opposite effect. This course can be clearly observed at the 480 nm maximum, while there are only mild effects of the treatments visible at 400 nm. This behaviour, with highest fluorescence intensity at the blue peak was almost identically observed in previous studies (Hanson et al., 2004) for roGFP1.

When comparing the steady states (blue curves) of the two sensor versions it is apparent that the ER-targeted version (Figure 5B) is highly oxidised, closely following the trajectory of the H_2O_2 curve, whereas the cytosolic version (Figure 5A) is in a more reduced state. This reflects the differences in the redox environment of the two compartments, thus indicating the correct localisation of the sensors. Although ER-roGFP displays a higher fluorescence intensity than cyto-roGFP at shorter wavelengths, which resembles the behaviour of the oxidised sensor, both steady states leave the corridor between the spectra of maximal reduction and oxidation there. This may be due to the relatively low sensitivity of the plate reader measurement, as this method does not detect single cells, but only the overall fluorescence in a well, which may be diluted by untransfected cells. It is also possible that the treatments have some effects on the autofluorescence of the cells, hence affecting the measured intensities in this range.

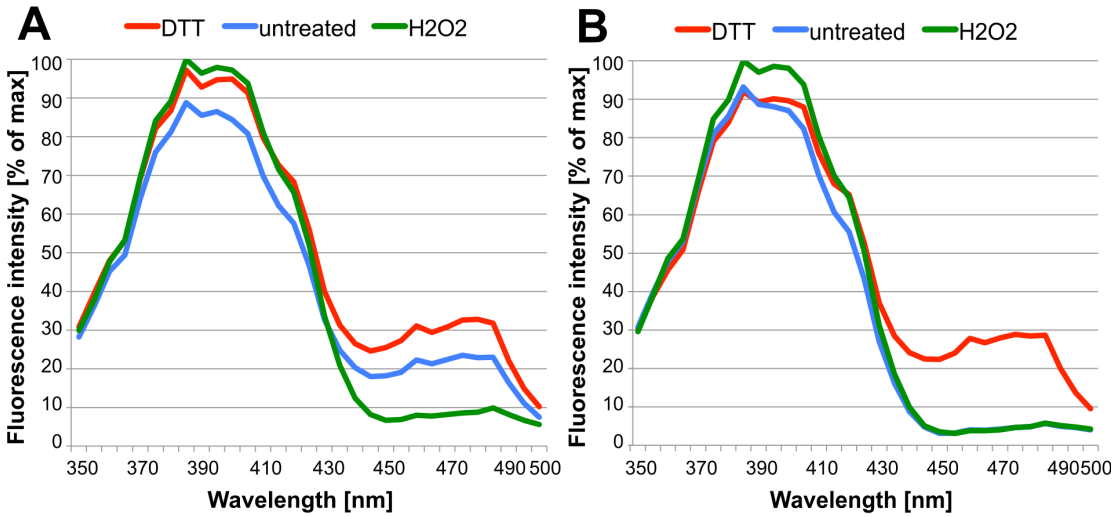

Figure 5: Excitation spectra of cyto-roGFP (A) and ER-roGFP (B). The average intensities of triplicate measurements are shown as percentages of the maximum intensity. Untransfected cells were used as blanks. The intensities of the two excitation maxima at approximately 400 nm and 480 nm strongly depend on the redox states of the sensors. Hence, the untreated state (blue curve) of the cytosolic version (A) differs from the ER-directed version (B) in relation to the oxidised (red curve) and reduced (green curve) states.

The measured excitation spectrum of HyPer (Figure 6) are also in agreement with previous findings (Birk et al., 2013), with the two excitability maxima at 420 nm and 500 nm. Here, the treatments have the exact opposite effect compared to roGFP, with oxidation increasing the intensity at larger wavelengths and decreasing it at shorter wavelengths.

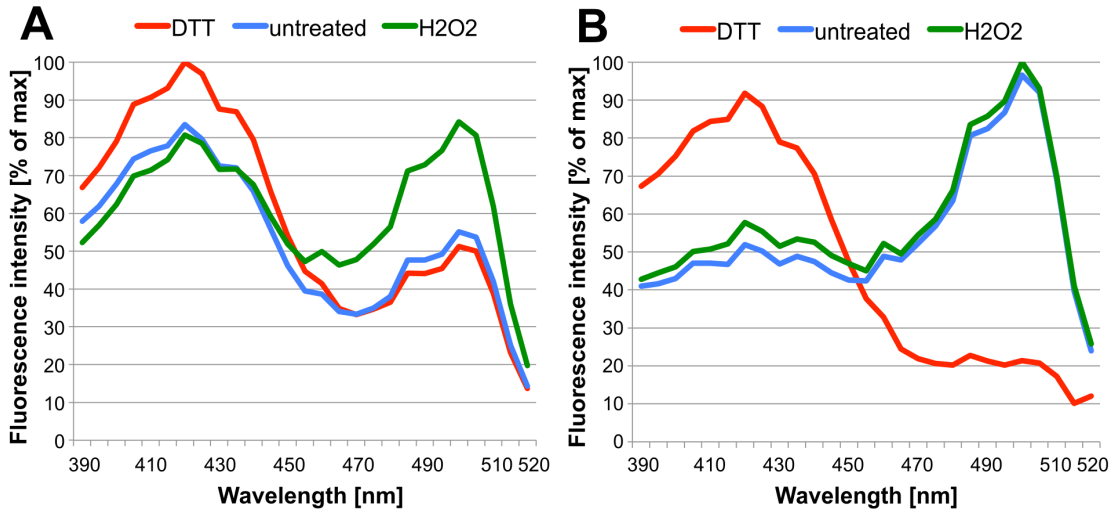

Figure 6: Excitation spectra of cyto-HyPer (A) and ER-HyPer (B). The average intensities of triplicate measurements are shown as percentages of the maximum intensity. Untransfected cells were used as blanks. The two excitation maxima at approximately 420 nm and 500 nm shift depending on the redox state of the sensor. The untreated state (blue curve) of the cytosolic version (A) differs from the ER-directed version (B) in relation to the oxidised (red curve) and reduced (green curve) states.

Again, the steady states (blue) of the two sensor versions clearly reflect the expected redox environments. ER-HyPer (Figure 6B) follows an almost

identical path as the H_2O_2 curve (green), whereas cyto-HyPer (Figure 6A) closely tracks the DTT curve (red) at larger wavelengths. Interestingly, the same tendency of the steady states toward lower intensities at shorter wavelengths as with roGFP is observed. As for roGFP, the steady states expose the expected behaviour relative to each other with cyto-HyPer showing higher intensities (above the H_2O_2 curve) than ER-HyPer (below the H_2O_2 curve).

In summary, we could reproduce the published excitation spectra of roGFP and HyPer, although we observed lower fluorescence intensities for the steady states at shorter wavelengths. Also, the difference in the steady state spectra of the two versions of the sensors clearly reflects the different redox states in the target compartments.

1.2. Localisation of the redox sensors

To directly confirm the correct localisation of the two compartment specific versions of the redox sensors we analysed cells expressing the sensors using immunofluorescence microscopy. For this purpose, the ER was stained with an antibody against the ER marker protein ERp57 (shown in red). Since the sensors both emit blue and green light, they were detected using a 405 nm and 488 nm laser with the band pass filters AmCyan1 and EGFP respectively.

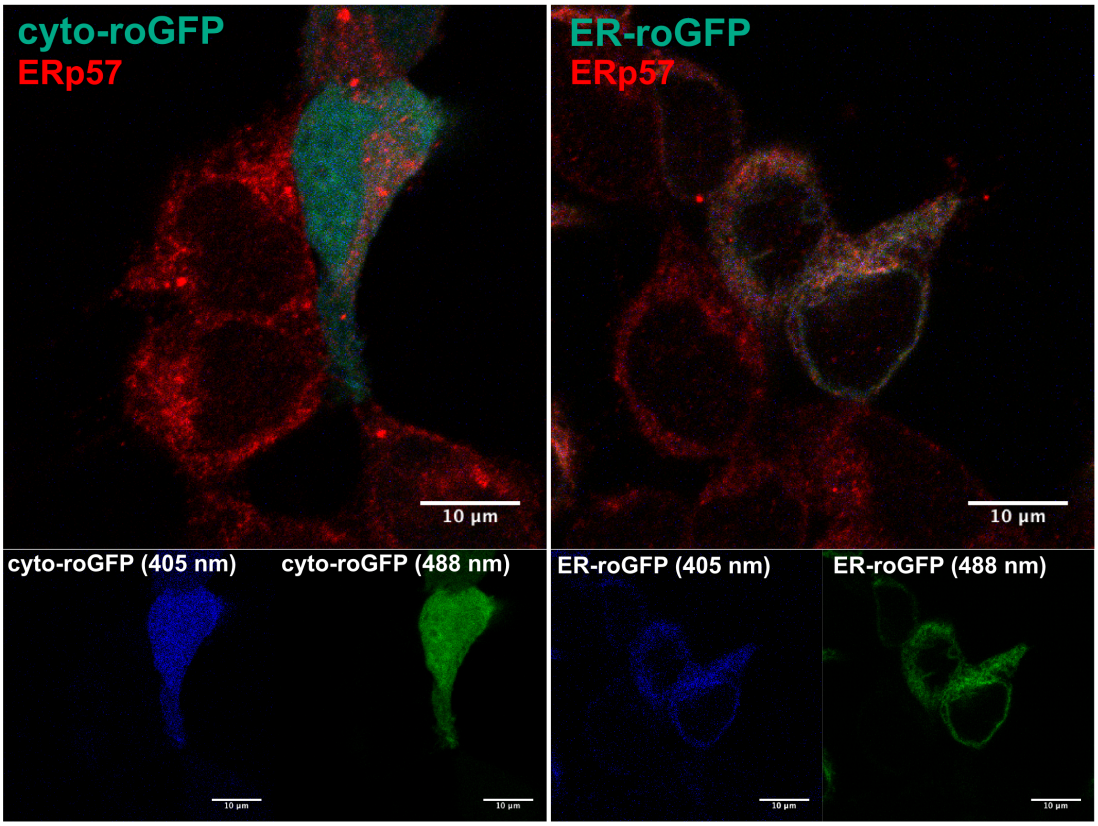

Figure 7: Localisation of the two compartment specific versions of roGFP using immunofluorescence microscopy. The fluorescence of the sensors was detected with the AmCyan1 and EGFP filters and is hence shown in blue and green, respectively. The images from the two channels are displayed separately in the bottom images. The ER, shown in red, was stained with an antibody against ERp57 and a Cy3 conjugated secondary antibody.

The overlay images (Figure 7) clearly show that the cytosolic roGFP (left) is uniformly distributed throughout the cell and does not colocalise with the ER marker. In contrast, the ER-targeted roGFP (right) fully colocalises with the ER marker.

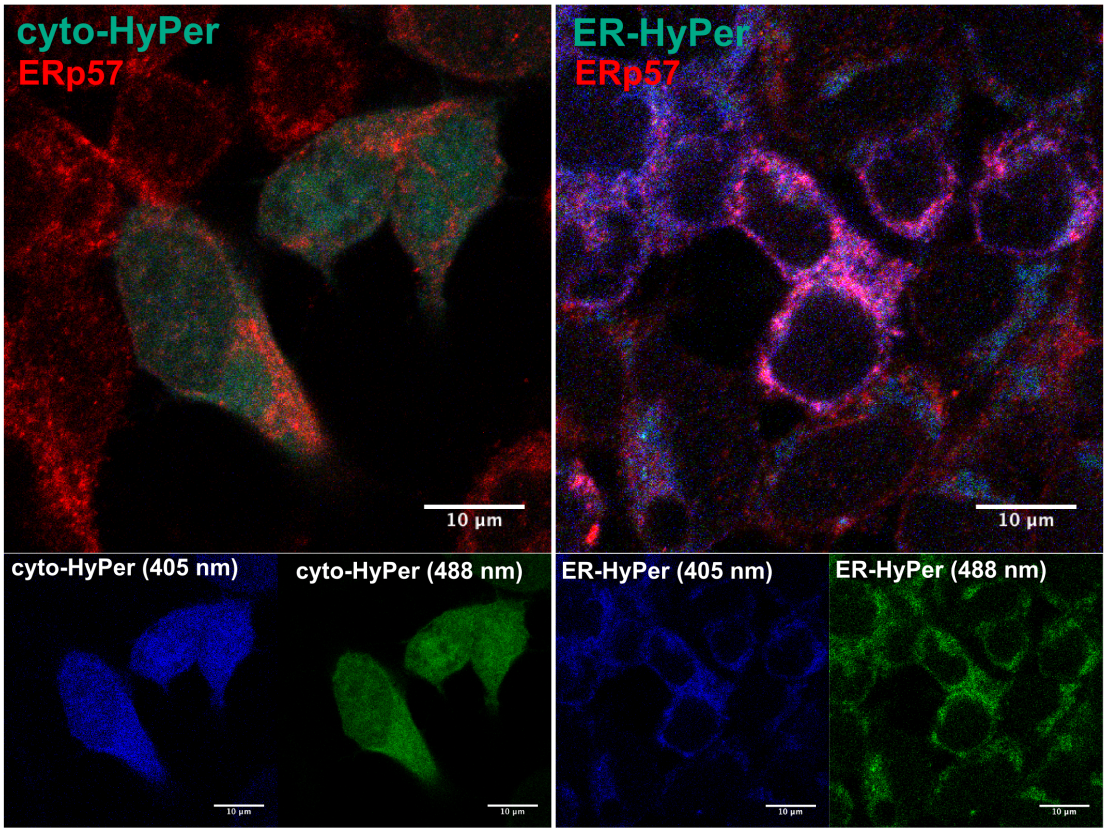

Figure 8: Localisation of the two compartment specific versions of HyPer using immunofluorescence microscopy. The fluorescence of the sensors was detected with the AmCyan1 and EGFP filters and is hence shown in blue and green, respectively. The images from the two channels are displayed separately in the bottom images. The ER, shown in red, was stained with an antibody against ERp57 and a Cy3 conjugated secondary antibody.

The same result can be seen for the HyPer sensors in Figure 8. However, the cytosolic versions also localises to the nucleus and other compartments. Nevertheless, the redox environment in the nucleus and most other cellular compartments is very similar to that of the cytosol, which was also observed in a study with HyPer (Malinouski et al., 2011). Thus, this possible unspecificity of the cytosolic sensors regarding the reported redox environment can be neglected. One option to prevent the arbitrary exchange of the protein between the cytosol and the nucleus would be to fuse a specific signal peptide to the sensor.

In summary, the microscopic analysis clearly confirms that the sensors are correctly localised and hence we can assume that they specifically report the redox environment of their target compartments.

1.3. FACS data processing

All subsequent measurements of the fluorescence intensities of the redox sensors were obtained by FACS analysis because of the high precision of this method as it measures individual cells and allows the analysis of a large number of events. Even though the excitation peaks of HyPer do not meet the standard wavelengths 405 nm and 488 nm as precisely as the roGFP maxima, we used these standard lasers for the detection of both sensors with the fluorescence activated cell sorter (FACS). The filter AmCyan was applied to gather emission between 485 nm and 535 nm and the FITC filter for fluorescence emission between 515 nm and 545 nm for excitation with the 405 nm and 488 nm lasers respectively.

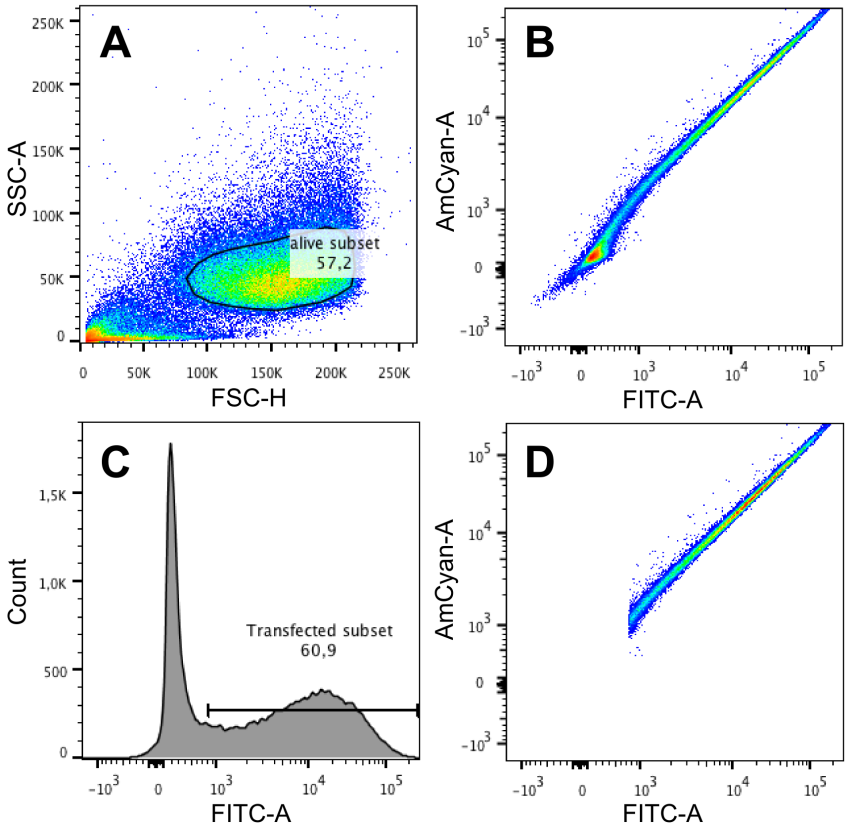

Figure 9: Example data processing of FACS measurements. Gating for living cells (A) and for transfected cells (C) lead to the scatterplots (B) and (D) respectively, which display the fluorescence intensities of each selected cell in the measured filters FITC (530/30) and AmCyan (510/50) (see below for details).

FACS data were analysed with the software FlowJo following four steps:

1. Living cells were gated manually in the FSC-H/SSC-A scatterplot of one sample (Figure 9A). Living cells are characterised by medium FSC values and low SSC values, corresponding to their average cell size and low granularity. The gate was applied to all samples.
2. A second gate was defined to select the transfected cells, which have higher fluorescence intensity in the FITC-A channel than untransfected cells and thus make up the right hand peak in the histogram (Figure 9C). This gate was again applied to all samples.

3. The mean fluorescence intensities in both channels (FITC and AmCyan) of all live and transfected cells were calculated for each sample.
4. The ratio of the mean fluorescence intensities was calculated as $I_{405\ nm}/I_{488\ nm}$ for roGFP probes and as $I_{488\ nm}/I_{405\ nm}$ for HyPer probes to compensate the opposing behaviour of the excitation spectra and thus allowing the same interpretation of the relative values of the ratios.

To allow for ratiometric analysis the cells must be on a straight line with gradient 1 in the FITC-AmCyan-scatterplot, which is shown in Figure 9D. For differing plots a ratiometric analysis would not be possible because this would mean that the ratio varies strongly between cells.

To test the variability of the sensors we analysed the distribution of the ratios of all individual transfected cells in one sample (usually about 40,000) (Figure 10).

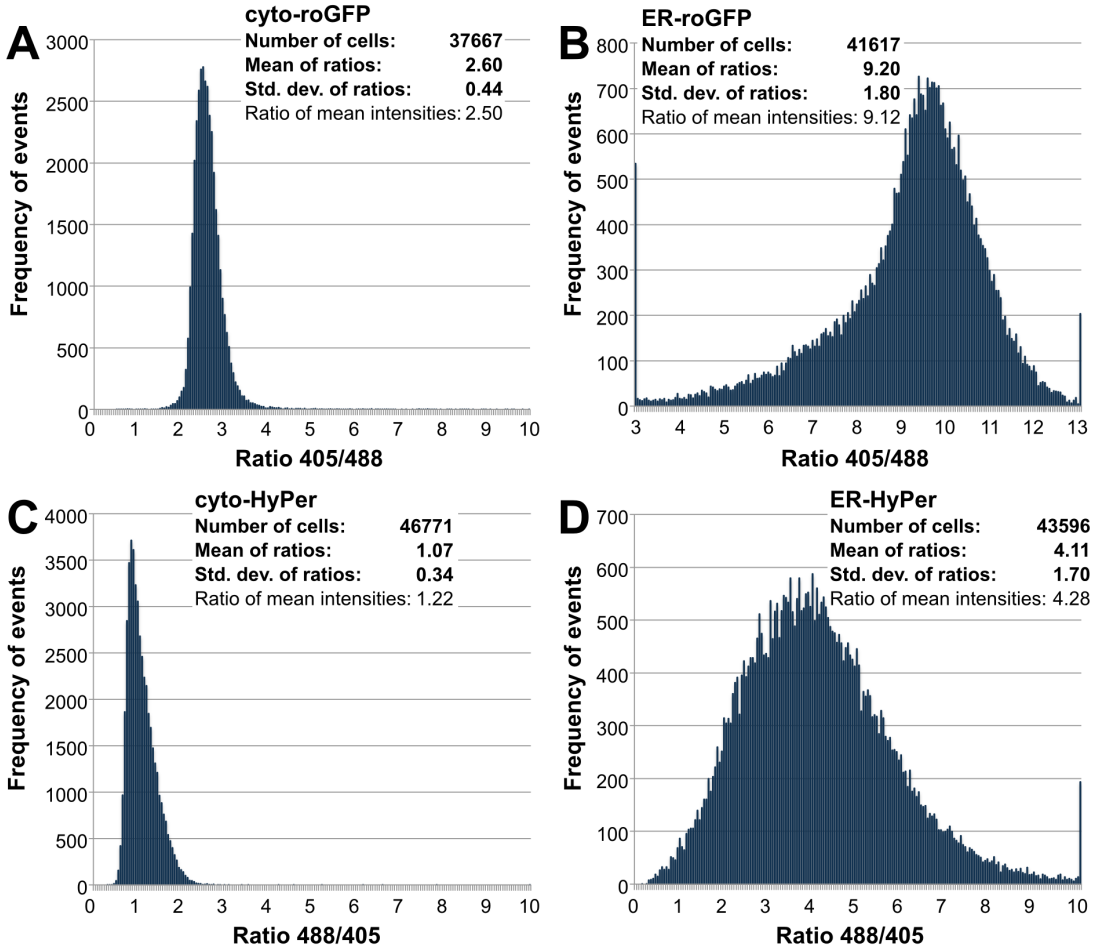

Figure 10: Distributions of the fluorescence intensity ratios of cells transfected with cyto-roGFP (A), ER-roGFP (B), cyto-HyPer (C) and ER-HyPer (D). The mean of the ratios of all individual cells in one probe (Mean of ratios) as well as the corresponding standard deviation (Std. dev. of ratios) is displayed in the legend and compared to the ratio of the mean fluorescence intensities in the two channels of a probe (Ratio of mean intensities).

Interestingly, the cytosolic versions of both sensors show considerably less variability than the ER-targeted versions, which is clearly displayed in the

standard deviations of the ratios (given in the insets). Thus, the measurements of ER-versions are expected to be less precise. This is especially the case for ER-HyPer, where the standard deviation is large relative to the mean of the ratios. However, because of the large number of individual events measured in a FACS analysis, the resulting mean of the ratios is very accurate, even if the ratio of single events varies.

Thus, alternatively to step 4 in the data analysis procedure, one could calculate the mean of all ratios instead of the ratio of mean intensities, as they should be identical for a ratiometric sensor. Indeed only marginal differences were observed for the example data (Figure 10).

1.4. Determination of the dynamic range

The steady state of the sensor in a given experiment can be rated in proportion to the maximally reduced and oxidised states and in this way compared to results from other experiments. Thus, the conditions for maximal reduction and oxidation had to be determined. For this purpose, cells were treated with varying concentrations of the redox agents diamide and H_2O_2 for oxidation and DTT for reduction and measured by FACS after the indicated time of incubation. The time points were chosen in the range of a few minutes; long enough to allow sufficient diffusion of the agent through the cellular membranes into the cytoplasm and ER and short enough to prevent depletion of the toxic substances via cellular defence mechanisms.

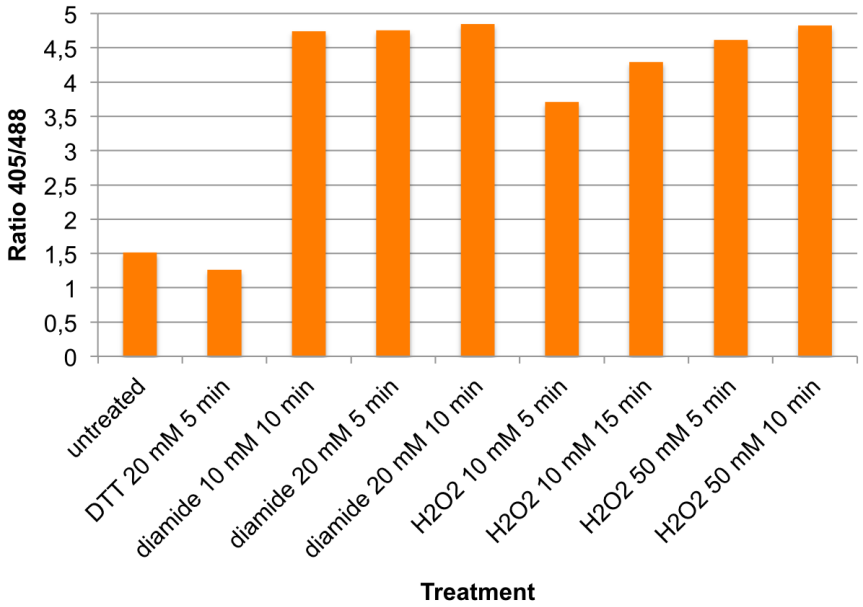

Figure 11: Effects of redox agents on cyto-roGFP. Transiently transfected cells were treated with the oxidising agents diamide and H_2O_2 or the reducing agent DTT at different concentrations and incubated for the specified time periods before they were analysed using FACS to determine the conditions for maximal reduction and oxidation of the sensor.

roGFP was maximally reduced (lowest ratio) with 20 mM DTT after 5 min incubation and fully oxidised (highest ratio) with either 20 mM diamide or 50 mM H_2O_2 after 10 min (Figure 11). In another experiment (data not shown)

it was confirmed that a higher concentration of DTT did not achieve further reduction.

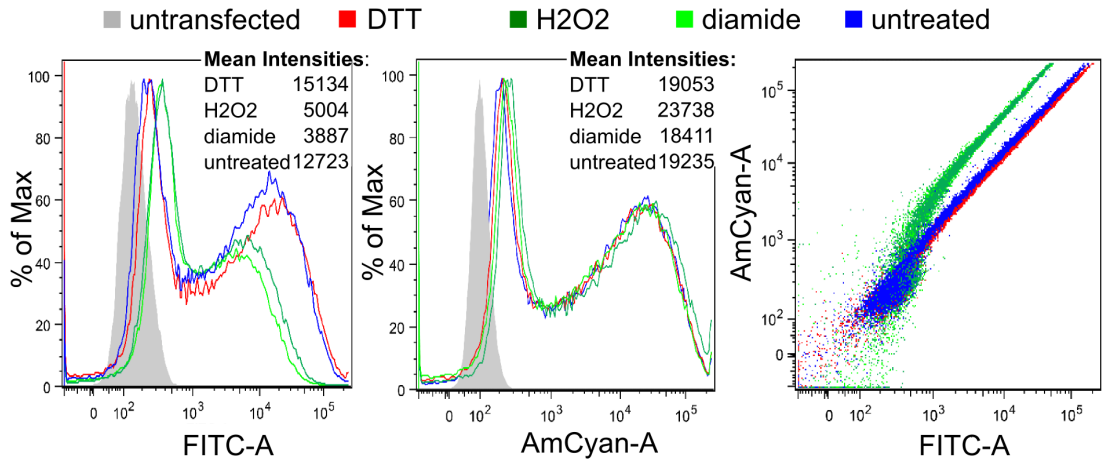

Figure 12: Effects of redox agents on cyto-roGFP displayed in the channel specific (FITC, AmCyan) distributions of the measured fluorescence intensities and in the corresponding scatterplot. The left peak (grey) in the histograms corresponds to the untransfected cells in the probe and the right peak to the transfected cells. Mean fluorescence intensities are only based on the transfected cells.

Interestingly, the changes in the ratios upon oxidation and reduction were mainly caused by a shift of the fluorescence intensity in the FITC channel (Figure 12). This observation agrees with the excitation spectra obtained with the plate reader (see III.1.1), where also only marginal changes in the blue range fluorescence intensities upon treatments were observed. The shifts in the FITC channel (left chart), however, clearly reflect the sensor's characteristic behaviour. The decrease of excitability at 488 nm due to oxidation is displayed in a shift to the left towards lower intensities (green curves), while DTT (red curve) leads to a shift towards higher intensities, reflecting the increased excitability upon reduction.

HyPer was maximally reduced with 40 mM DTT after 5 min (Figure 13). However, 10 mM and 20 mM DTT almost reached the same ratio. Thus, 10 mM DTT was used in further experiments to minimise possible toxicity. Full oxidation could be achieved with a significantly lower concentration of H_2O_2 than for roGFP, reflecting the high sensitivity of HyPer to H_2O_2. Interestingly, in contrast to the treatment of roGFP with H_2O_2, for HyPer we observed a rapid decrease of the ratio with increasing H_2O_2 concentrations and incubation time, even below the initial steady state ratio. This effect was also observed in previous studies (Malinouski et al., 2011) and was suggested to be due to partial bleaching of the cells or due to an overshooting activity of H_2O_2 scavenging systems as a cellular response to H_2O_2 leading to a reduction of the H_2O_2 concentrations below physiological values. Remarkably, roGFP, the sensor for detection of the main cellular redox buffer GSH/GSSG, does not show this behaviour even with much higher H_2O_2 concentrations. Therefore, another explanation for the divergent effect of H_2O_2 could be that the chromophore system of HyPer is so sensitive to H_2O_2 that it is readily destroyed, but that the agent does not have a destructive effect on the roGFP chromophore.

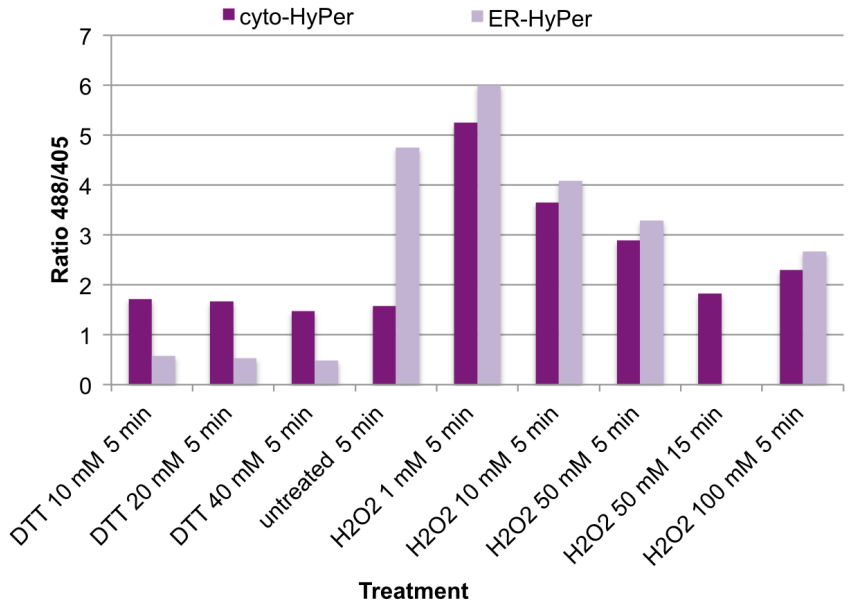

Figure 13: Effects of redox agents on HyPer. Transiently transfected cells were treated with the agents H_2O_2 and DTT at different concentrations and incubated for the specified time periods before they were analysed using FACS to determine the conditions for maximal reduction and oxidation of the sensor.

The channel specific behaviour of HyPer (Figure 14) clearly shows the expected shifts in the fluorescence intensities upon a change in the redox state with an opposing trend in the FITC and AmCyan channel. In contrast to roGFP, the shifts are in opposite direction, which clearly demonstrates how the switch in the green and blue fluorescence is exactly opposite in the two sensors.

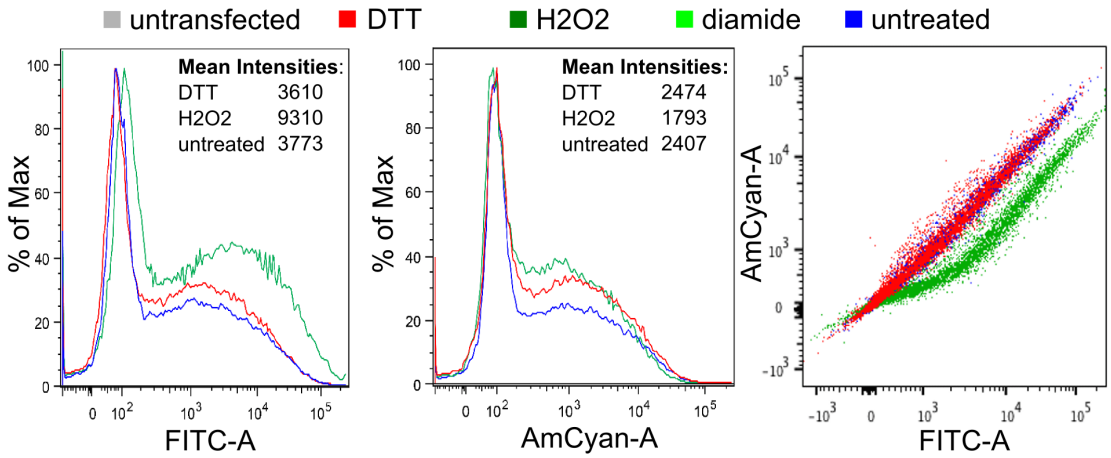

Figure 14: Effects of redox agents on cyto-HyPer displayed in the channel specific (FITC, AmCyan) distributions of the measured fluorescence intensities and in the corresponding scatterplot. The left peak in the histograms corresponds to the untransfected cells in the probe and the right peak to the transfected cells. Mean fluorescence intensities are based on transfected cells only.

However, the HyPer chromophore shows shifts in both channels (which is also consistent with the obtained excitation spectra), whereas the shifts in the roGFP fluorescence mainly occurred in the FITC channel. This might

negatively affect the ratiometric quality of roGFP and the major advantage of the ratiometric redox sensors, the independence from sensor concentration, as there seems to be no opposing shift at the second excitation peak. Therefore, it is necessary to confirm the ratiometric behaviour of the sensors before using them for further experiments (see next chapter).

In conclusion, the conditions for maximal oxidation and reduction of the sensors were determined and the ratio of florescence intensities was established as an examination method of the FACS data, correctly displaying the redox states of the sensors.

1.5. Confirming the detection of compartment specific redox states

Next, we wanted to confirm that the sensors correctly report their redox environment (as already indicated by the plate reader measurements) in the ratios of mean fluorescent intensities obtained by FACS analysis and in a Western blot.

The steady state ratios of the two roGFP versions (cyto-roGFP and ER-roGFP) (Figure 15A) clearly show the difference in the redox environment of the two compartments, with the ratio of the ER-targeted sensor about four times higher than that of cyto-roGFP. The untreated cytosolic roGFP appears to be almost fully reduced, whereas the ER-version is oxidised. Both variants could be further reduced and oxidised with redox agents (Figure 15). The same observations were made for both HyPer versions (Figure 15B). Hence, we successfully established the ratiometric behaviour of all four sensors.

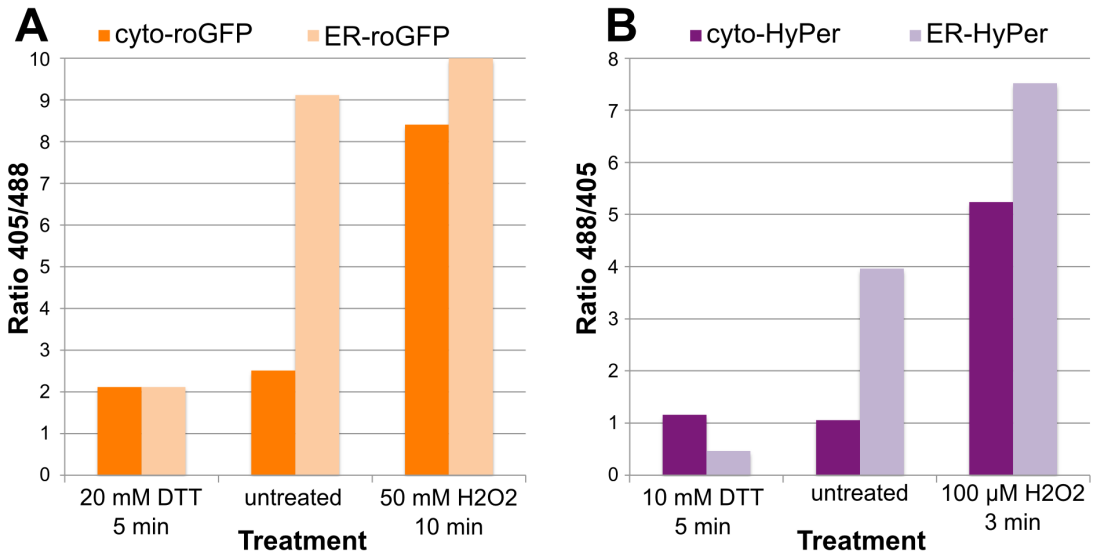

Figure 15: Comparison of the compartment specific versions of roGFP (A) and HyPer (B). The large difference in the ratios of the two versions reflects the different redox states of the cytosol and the ER. To judge the scale of these ratios the fully reduced and oxidised ratios are also displayed.

The two versions of the sensors are not entirely comparable, however, since the same treatments lead to different reduction and oxidation values. This effect is particularly pronounced for the treatment with H_2O_2. Similarly, a much stronger reduction of ER-HyPer than of cyto-HyPer is achieved with DTT. Thus, the ER-targeted sensor reacts more sensitively. This may be explained

by an effect of the attached signal peptide on the chromophore or by the ER somehow absorbing the added reagents leading to higher local concentrations there. The first explanation seems relatively unlikely as both HyPer and roGFP, two different proteins with different chromophore systems, display this effect. Since the ER is highly involved in several redox interactions the latter seems more plausible. Furthermore, HyPer and roGFP show different sensitivities to the treatments, especially to H_2O_2. This is not surprising since roGFP is an indirect sensor of the redox potential through the GSH/GSSG equilibrium, while HyPer directly reacts with H_2O_2 (for a detailed explanation of the mechanisms see I.5.2).

The source of the ratio changes can be seen in the shifts of the mean fluorescence intensities of the two channels (Figure 16). Here, we can clearly see the divergent course of the absolute fluorescence signals (and their inverse behaviour for the two sensors) causing a change of the ratio upon an alteration of the redox environment.

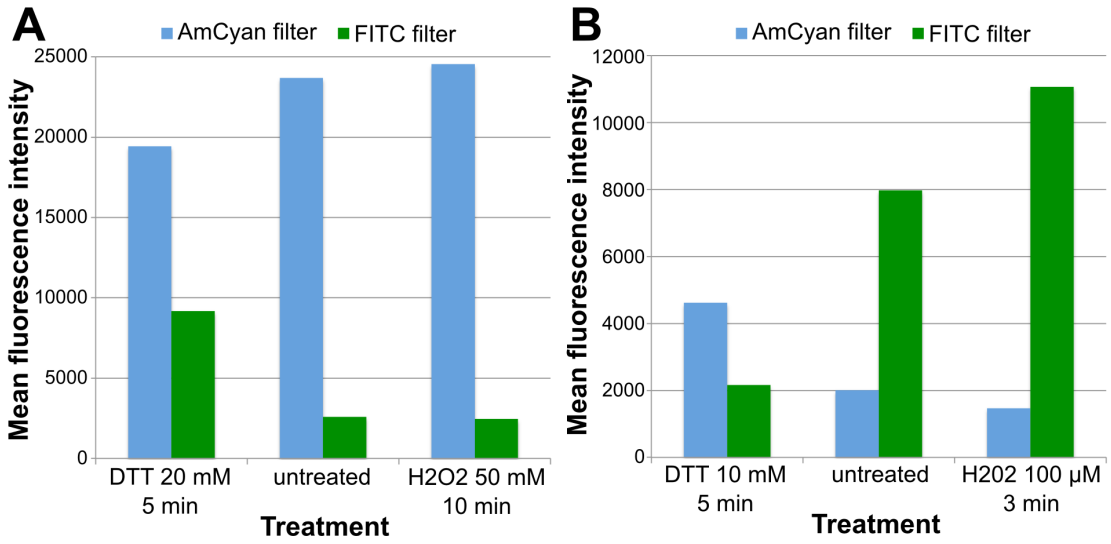

Figure 16: Channel specific effects of the redox agents on cells transfected with ER-roGFP (A) and ER-HyPer (B). The sensors show an inverse behaviour of the mean fluorescence intensities in the FITC (green) and AmCyan (blue) channel upon oxidation. The same result was observed for the cytosolic versions of the sensors.

To complement the observations made in the FACS analysis with a biochemical validation of roGFP, cell lysates were analysed in a reducing and non-reducing gel electrophoresis on bis-tris gels followed by Western blotting and subsequent detection using an anti-GFP antibody (Figure 17). On both gels the main band at 27 kDa confirms the expression of roGFP. The band below may either come from an unspecific interaction of the antibody or a fragment of roGFP. The non-reducing gel (right) clearly shows the difference between the oxidised (ER-roGFP) and reduced (cyto-roGFP) states of the sensor in the presence of bands above the main band of roGFP at 27 kDa. These could be explained by the formation of intra- and possibly also intermolecular disulphide bonds leading to conformational changes and oligomer formation respectively. These disulphide bonds cannot be formed with reduced cysteines and thus the bands do not appear in the lanes of cyto-roGFP from untreated cells and post-lysis reduced (with DTT) cyto-roGFP as

well as in the control reducing gel (left). In ER-roGFP from cells treated with DTT these higher bands are weaker than in the untreated and oxidized ER-roGFP, however they did not fully disappear, indicating that the reducing treatment may not have been strong enough or ER-roGFP was rapidly re-oxidised in the ER after removing the treatment. ER-roGFP from untreated cells and both roGFP variants from cells treated with H_2O_2 display the multimeric bands. Thus, the steady states of the compartment specific sensors reflect the expected redox environment. Furthermore, the treatments with the redox agents clearly shifted the redox state of the sensors in the expected directions.

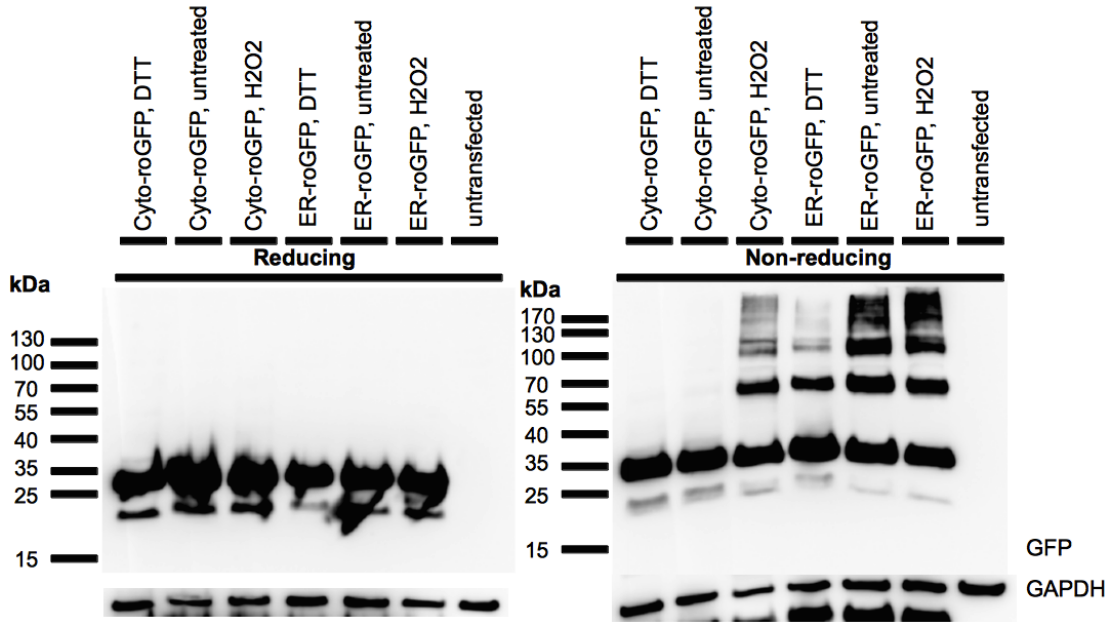

Figure 17: Reducing (left) and non-reducing (right) western blot showing the different redox states of cyto-roGFP and ER-roGFP. roGFP was detected with an anti-GFP antibody. The fully oxidized (from cells treated with 50 mM H2O2) and reduced (from cells treated with 20 mM DTT) sensors are used as controls. GAPDH serves as loading control.

In summary, both in the ratio analysis and in the Western blot analysis the compartment specific redox sensors correctly report their redox environment.

1.6. Confirming functionality of the ratiometric analysis

The ratiometric behaviour of the redox sensors, i.e. the proportionality of the fluorescence intensity signals in the two channels, should make the measured ratios independent of the sensor concentration and bleaching effects. To confirm this, we compared the ratiometric measurement results of the sensors expressed at different concentrations. For this purpose, we transfected cells with two concentrations of sensor plasmid DNA. Since the transfection protocol was optimised for a certain amount of DNA, we used this amount for a single transfection. For a lower expression level we replaced half of the sensor plasmid with the empty vector pcDNA3.1 in a cotransfection. As a result, the amount of sensor expressed in the latter should be about half. Additionally, to simulate co-expression with another protein, which might have different effects on the cells to those of an empty vector, as it requires the

overexpression of an additional protein, we transfected cells with the sensor and the α protein. This protein has the additional advantage of being a negative control for the β proteins as it has a similar amino acid composition but remains completely soluble when expressed in cells.

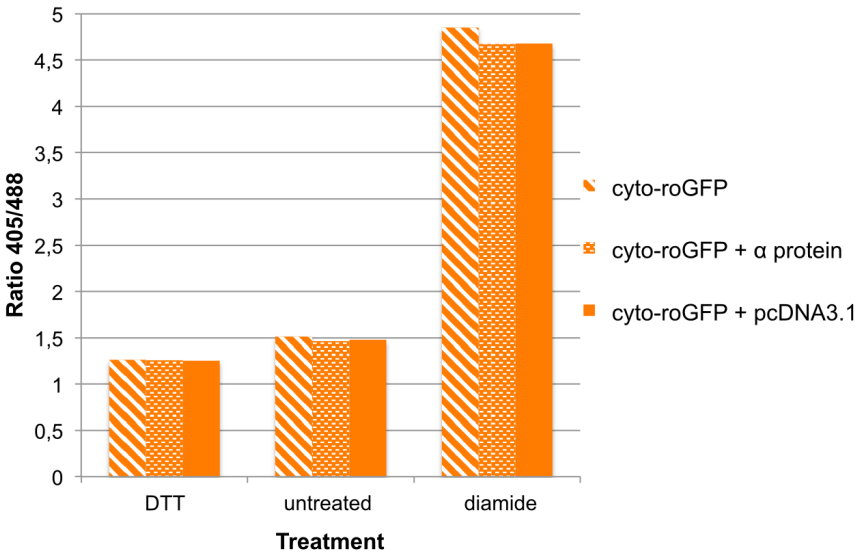

Figure 18: Influence of sensor concentration and cotransfection on the ratios of roGFP. A single transfection (cyto-roGFP) was compared to a transfection with half the amount of plasmid (cyto-roGFP + pcDNA3.1). Additionally, the effects of cotransfection with a soluble protein (cyto-roGFP + α protein) were analysed.

Figure 18 clearly shows that the ratios obtained with roGFP are independent of the amount of roGFP plasmid transfected and thus, the cellular concentration of roGFP.

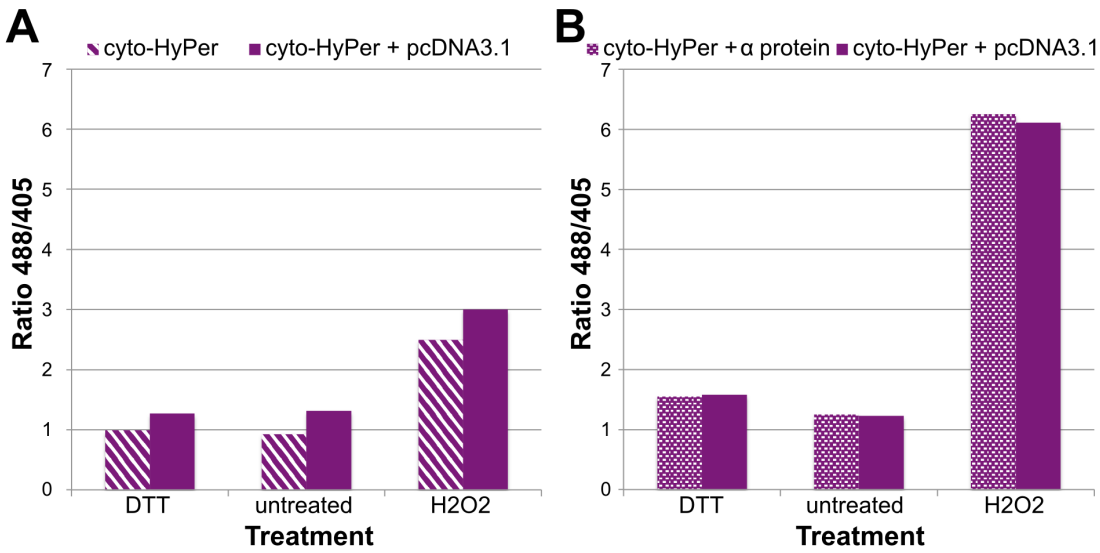

Figure 19: Influence of sensor concentration (A) and cotransfection (B) on the ratios of HyPer. (A) A single transfection (cyto-HyPer) was compared to a transfection with half the amount of plasmid (cyto-HyPer + pcDNA3.1). (B) The effect of cotransfection with a soluble protein (cyto-HyPer + α protein) was also analysed.

The ratiometric behaviour of HyPer in contrast showed a slight dependence on the sensor's expression level (Figure 19A). This could be explained by the slightly greater distance of HyPer's excitation maxima (420 nm, 500 nm) from the used standard wavelengths (405 nm, 488 nm) than those of roGFP (400 nm, 480 nm), so that the influences of the fluorescence shifts are somewhat distorted in the ratio. However, cotransfection with a protein instead of an empty vector did not influence the redox sensing behaviour of roGFP (Figure 17) or HyPer (Figure 19B). Hence, the functionality of the ratiometric behaviour of the sensors is demonstrated.

1.7. Effects of treatments on untransfected cells

To exclude the possibility that the ratio changes upon treatment with DTT and H_2O_2 are an indirect effect of these chemicals, independent of the redox sensors, we analysed untransfected cells after the treatments (Figure 20).

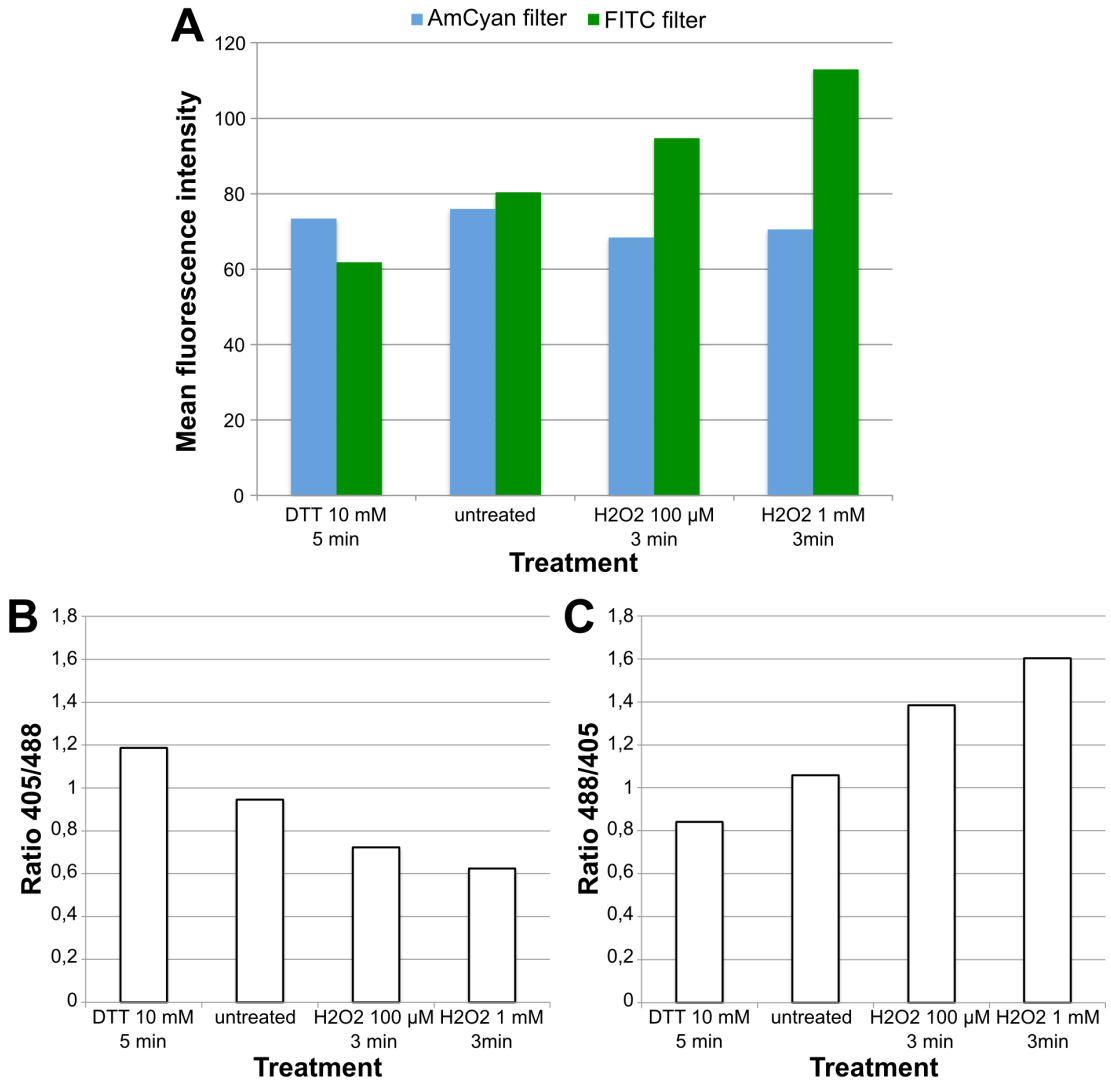

Figure 20: Effects of the redox agents on the fluorescence intensities (A) of untransfected cells and the resulting ratios $I_{405\ nm}/I_{488\ nm}$ (B) and $I_{488\ nm}/I_{405\ nm}$ (C). The autofluorescence of untransfected cells was analysed after treatments similar to those of cells transfected with the sensors. For comparison with the data derived from sensor transfected cells, the ratio $I_{405\ nm}/I_{488\ nm}$ used for roGFP analysis (A) and the inverse ratio $I_{488\ nm}/I_{405\ nm}$ used for HyPer analysis (B) are shown.

Notably, we could observe shifts in the FITC channel upon treatments with H_2O_2 and DTT, but the fluorescence signal in the AmCyan channel remained constant (Figure 20A). In particular, H_2O_2 has a marked and concentration dependent influence on the green fluorescence signal displayed in an increase of more than 40 % for 1 mM H_2O_2. However, compared to the wavelength specific effect of the same treatments on cells expressing roGFP or HyPer (see Figure 16), the magnitude of these changes is minimal.

The reason for the observed changes in the green autofluorescence of untransfected cells could be alterations in the cellular form, granularity or membrane integrity induced by the redox agents as it is well known that they are toxic. Such structural details are normally distinguished in the forward and side scatter measurements by FACS. But they could potentially also show up in the minor autofluorescence of the cells.

Figures 20 B and C show the ratios used for analysis of roGFP ($I_{405\ nm}/I_{488\ nm}$, B) and HyPer ($I_{488\ nm}/I_{405\ nm}$, C) calculated for the untransfected cells. Here, the observed changes in the FITC channel emerge, leading to the same trend of increasing ratios with an increasing oxidation state as it appears for HyPer, but opposing the trend of roGFP. Thus, one could argue that the effects seen with HyPer are enhanced by this phenomenon and those for roGFP are reduced, especially since we used a considerably higher concentration of H_2O_2 for the oxidation of roGFP than we used with the untransfected cells. However, this is highly deceiving since the ratios are not additive. If correctly subtracting the absolute intensities from the intensities obtained with the sensors and calculating the ratio, the difference between this corrected ratio and the non-corrected one is only marginal (see example below).

$I_{488\ nm}/I_{405\ nm}$ (untransfected cells, H_2O_2 100 µM 3 min) = $\frac{94.7}{68.4} = 1.38$

Uncorrected $I_{488\ nm}/I_{405\ nm}$ (ER-HyPer, H_2O_2 100 µM 3 min) = $\frac{11071}{1472} = 7.52$

Corrected $I_{488\ nm}/I_{405\ nm}$ (ER-HyPer, H_2O_2 100 µM 3 min) = $\frac{11071-94.7}{1472-68.4} = 7.82$

Therefore, the effect of the treatments on the ratios, as a consequence of direct influences on the cellular autofluorescence and not on the redox environment, can be neglected.

2. Effects of β23 and sp-β23 on the redox potential

We analysed the effects of β23 and sp-β23 on the redox environment in the cytosol and the ER using both redox sensors. By conducting the experiment at two different time points after transfection, we investigated possible time dependent effects. In our analysis of possible error sources we confirmed the aggregation propensity of β23 and the correct localisation of all artificial proteins. Further, we excluded a direct effect of the β23 aggregates on the GFP chromophore.

2.1. Aggregation propensity of β23

To ensure that measurements of the effects of β23 on the cellular redox environment capture the aggregate toxicity we wanted to confirm that β23 actually formed aggregates with only half the amount of the protein expressed in a cotransfection with the redox sensor. For this purpose, we analysed transfected cells by immunofluorescence microscopy (Figure 21).

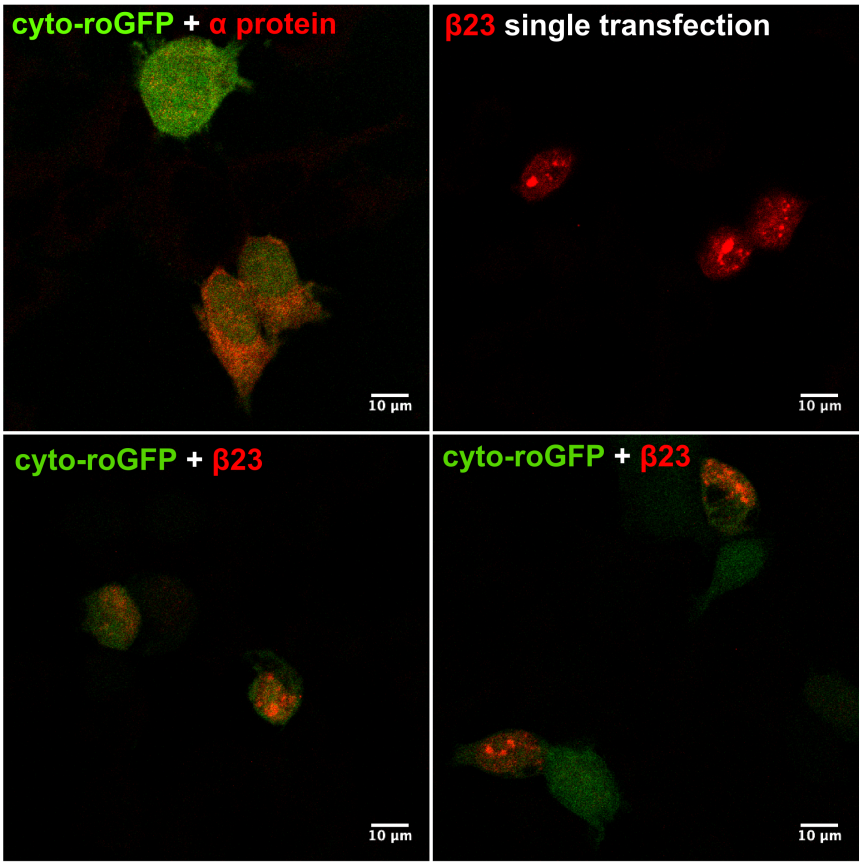

Figure 21: Analysis of the aggregation propensity of β23 cotransfected with cyto-roGFP by immunofluorescence microscopy. The fluorescence of the sensor was detected in the EGFP channel (green), while β23 and the α protein were detected with a Cy3 conjugated antibody (red). The bottom images show representative cells of β23 cotransfected with the sensor. The cotransfection with α protein as well as the β23 single transfection serve as negative and positive control, respectively.

The β protein was detected with a primary antibody against its Myc-tag and a secondary antibody coupled to the red fluorescent dye Cy3. As a positive control we used cells with β23 singe transfections, thus expressing the double amount of the protein that had previously been shown to form protein aggregates (Olzscha et al., 2011). A cotransfection of cyto-roGFP with the α protein served as negative control.

As expected, the soluble α protein was equally distributed throughout the cell and showed no aggregation. In contrast, cells transfected with the full amount of β23 showed several aggregates of varying sizes. The same phenotype was also observed with half the amount of DNA. These findings hence confirm that β23 forms aggregates both in cells transfected with the full amount of plasmid DNA and in those with only half the amount.

2.2. Localisation of the β proteins

Beside the aggregation propensity we verified the localisations of the artificial proteins used in the experiments by immunofluorescence microscopy (Figure 22).

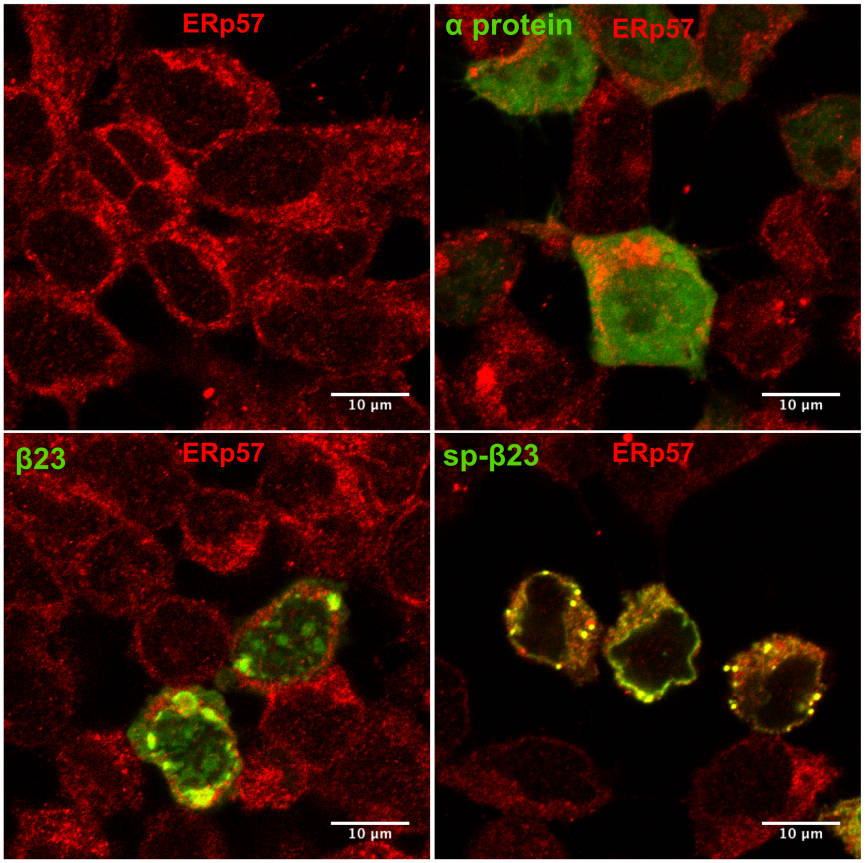

Figure 22: Localisation of the β proteins and the control α protein in the cell detected by immunofluorescence microscopy. The artificial proteins were detected with a Cy3 conjugated antibody binding the primary anti-Myc antibody and are here shown in green for consistency with the previous images. The ER, for consistency shown in red, was stained with an antibody against ERp57 and an Alexa Fluor 488 conjugated secondary antibody.

The ER was stained with an antibody against ERp57 (shown in red) and the overexpressed proteins (shown in green) were detected with antibodies against their Myc-tag. As expected, the control α protein is distributed uniformly throughout the cell, but does not colocalise with the ER, as it does not contain an ER-targeting signal peptide. Like the redox sensors, (see III.1.2), the α protein expressed in the cytosol also migrates into the nucleus. The same localisation is observed for β23, however, here we can clearly observe aggregation. This confirms the findings of the previous chapter.

Interestingly, β23 is mainly located around the nucleus. In contrast, sp-β23 fully colocalises with the ER marker, hence confirming its correct localisation and the functionality of the signal peptide. Although some foci can be observed, these also appear for the ER marker alone and can sporadically be seen in untransfeced cells as well. This would imply that the ER is extremely dense in some areas, occurring as foci in the microscopy images. It thus remains unclear, whether these foci are actually aggregates. Nevertheless, the microscopic analysis clearly confirms the correct localisations of the artificial proteins.

2.3. Effects of β23 on GFP

To exclude the possibility that β23 could directly affect the GFP chromophore and hence manipulate the sensor measurements, analysed the ratio changes in a cotransfection of β23 with GFP. Although the main excitation peak of GFP is at 475 nm, it has a second minor excitation peak at 395 nm. Hence when we used the standard excitation lasers, which we also used for the redox sensors, we received emission signals in both channels.

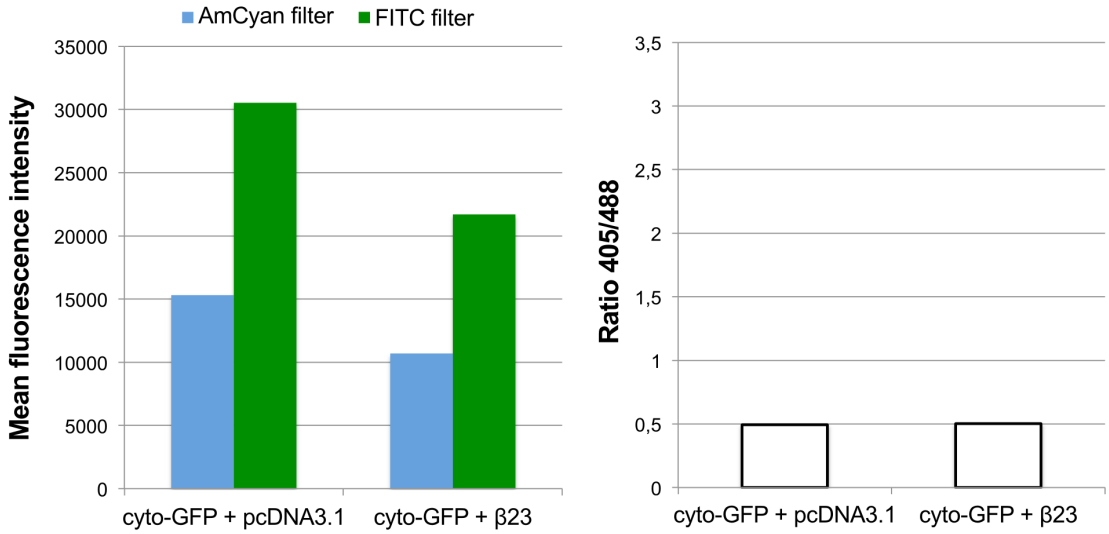

Figure 23: Effect of β23 on the fluorescence intensity signals of cytosolic GFP (left) and the ratio of the intensities (right). Cells cotransfected with cyto-GFP and β23 were compared to cells transfected with cyto-GFP and an empty vector. The mean fluorescence intensities were detected in the AmCyan and the FITC channels (left) and the corresponding ratios $I_{405\ nm}/I_{488\ nm}$ are shown on the right.

One has to keep in mind that the data for the two analysed GFP versions, cyto-GFP (Figure 23) and ER-GFP (Figure 24), were obtained using different laser settings, so the absolute intensities are not comparable. This also

explains why the blue fluorescence is greater than the green fluorescence for ER-GFP, since here the intensity of the 488 nm laser was set lower.

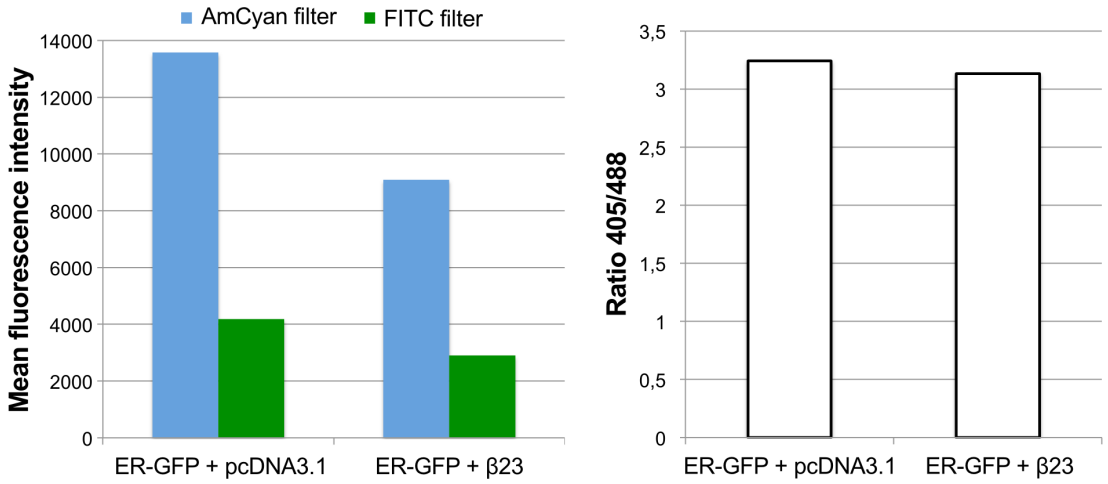

Figure 24: Effect of β23 on the fluorescence intensity signals of ER-targeted GFP (left) and the ratio of the intensities (right). Cells cotransfected with ER-GFP and β23 were compared to cells transfected with ER-GFP and an empty vector. The mean fluorescence intensities were detected in the AmCyan and the FITC channels (left) and the corresponding ratios $I_{405\ nm}/I_{488\ nm}$ are shown on the right.

Both GFP versions show a reduction in the mean fluorescence intensities when cotransfected with β23 (Figures 23 and 24). This could be explained by a reduction in the overall expression of GFP in cells cotransfected with another protein compared to the expression level in cells where an empty vector was cotransfected. β23 may also have an effect on the GFP structure, reducing the chromophores excitability. Nevertheless, since the intensity reduction is proportional in both channels, the effect is not reflected in the ratio ($I_{405\ nm}/I_{488\ nm}$) of the mean intensities. This is the case for both GFP versions. Therefore, we can conclude that a cotransfection of β23 with GFP does have an effect on the fluorescence intensities of the chromophore, but there is no effect in the ratiometric analysis.

Nevertheless, this experiment does not fully exclude an interaction of the β protein with the roGFP chromophore, since the mechanism of the roGFP chromophore is modified compared to the wild type chromophore. β23 may have an influence on the conformational change mechanism that reports alterations of the redox environment. To exclude this, one could perform an *in vitro* experiment with β23 and roGFP in a constant redox environment, analysing the effects on the ratio.

2.4. Cotransfection of the sensors with the β proteins

After confirming the localisation and functionality of the sensors, we applied them to examine the effects of amyloidogenic proteins on the cellular redox environments. To this end, we cotransfected the sensors with the artificial amyloidogenic protein β23 and its ER-targeted version sp-β23. As a negative control we used cotransfections of the sensors with an empty vector (pcDNA3.1) or the soluble α protein. Three independent repeats (n = 3) of this experiment were carried out using cyto-roGFP, cyto-HyPer and ER-HyPer and two independent repeats (n = 2) using ER-roGFP. To compare the results

of the independent experiments we normalised the ratios from all cotransfections for each experiment so that the ratio of the pcDNA3.1 cotransfection (which should have no effect on the sensors) was set to 1, since we are interested in the relative shifts of the β protein cotransfections. Then the mean and standard deviation of the normalised ratios were calculated for each cotransfection (Table 1).

Table 1: Mean and standard deviation (μ ± σ) of normalised ratios of cotransfections (pcDNA3.1, α protein, β23, sp- β23) with the four sensors

	pcDNA3.1	**α protein**	**β23**	**sp-β23**
cyto-roGFP	1.000 ± 0.000	0.997 ± 0.007	1.000 ± 0.010	1.009 ± 0.007
ER-roGFP	1.000 ± 0.000	1.006 ± 0.016	0.920 ± 0.016	0.944 ± 0.022
cyto-HyPer	1.000 ± 0.000	1.029 ± 0.021	0.831 ± 0.051	1.005 ± 0.039
ER-HyPer	1.000 ± 0.000	0.997 ± 0.176	0.886 ± 0.161	0.887 ± 0.119

For cyto-roGFP (Figure 25, left) the redox state measured by the sensor was almost equal for all cotransfections and the standard deviations were minimal. Hence, cyto-roGFP gives highly reproducible results, which do not show a change in the cytosolic redox environment upon cotransfection with the β proteins.

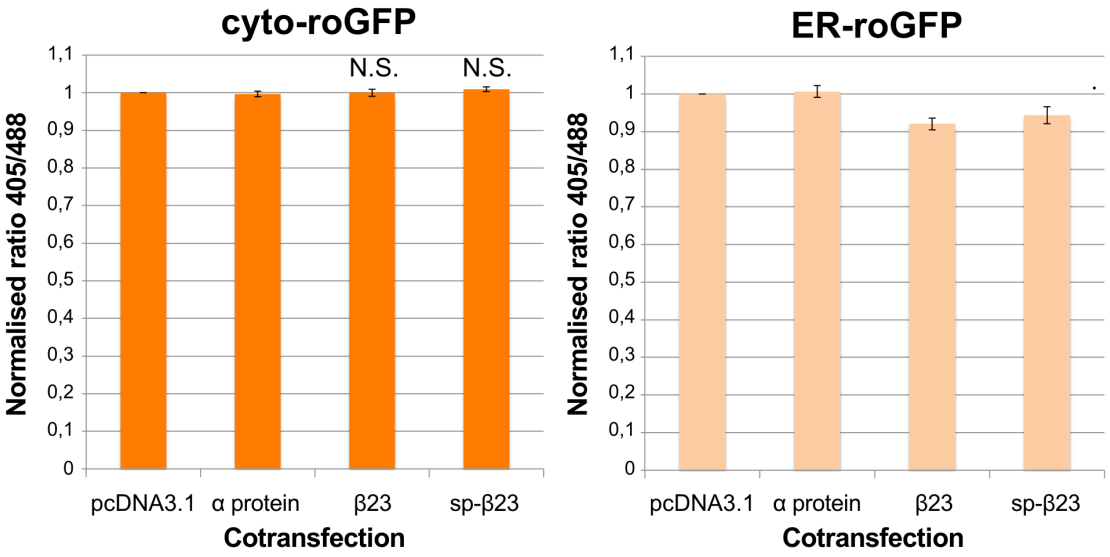

Figure 25: Effects of β23 and sp-β23 on the redox environment in the cytosol (left) and the ER (right) detected with roGFP. For comparison of independent repeats of the experiments the ratios were normalised to the pcDNA3.1 cotransfection. The mean and standard deviation of the normalised ratios are shown for cyto-roGFP (left) based on three independent experiments and for ER-roGFP (right) based on two independent experiments (hence no significance indicated). The cotransfections with pcDNA3.1 and α protein serve as negative controls. The significance of shifts in the ratios relative to the ratio of the α protein cotransfection is indicated by N.S. (p-value ≥ 0.1), * (p-value < 0.05), ** (p-value < 0.01).

In contrast, the ER-targeted variant of the sensor (Figure 25, right) displayed 8.5 % and 6.2 % reductions of the ratio when cotransfected with β23 and sp-β23, respectively, compared to the α protein. For β23 this gives a p-value of

0.058 and of 0.078 for sp-β23, which corresponds to a low presumption against the null hypothesis that the β proteins have the same effect on the mean ratio as the α protein. On a significance level of 90 % we can conclude that the observed ratio reductions are significant.

The same effect was seen with HyPer (Figure 26). Interestingly, here we could also detect a reducing effect of β23 with the cytosolic sensor (left). The effect was even more pronounced than seen with ER-roGFP with a reduction of 19.2 % and a p-value of less than 0.01, hence being highly significant. However, sp-β23 showed no effect on the ratio (with a p-value of 0.183). The ER-targeted HyPer also sensed a reduction of the redox environment for both β proteins, but due to the high standard deviations the effects are not significant (the p-values are about 0.3 for both).

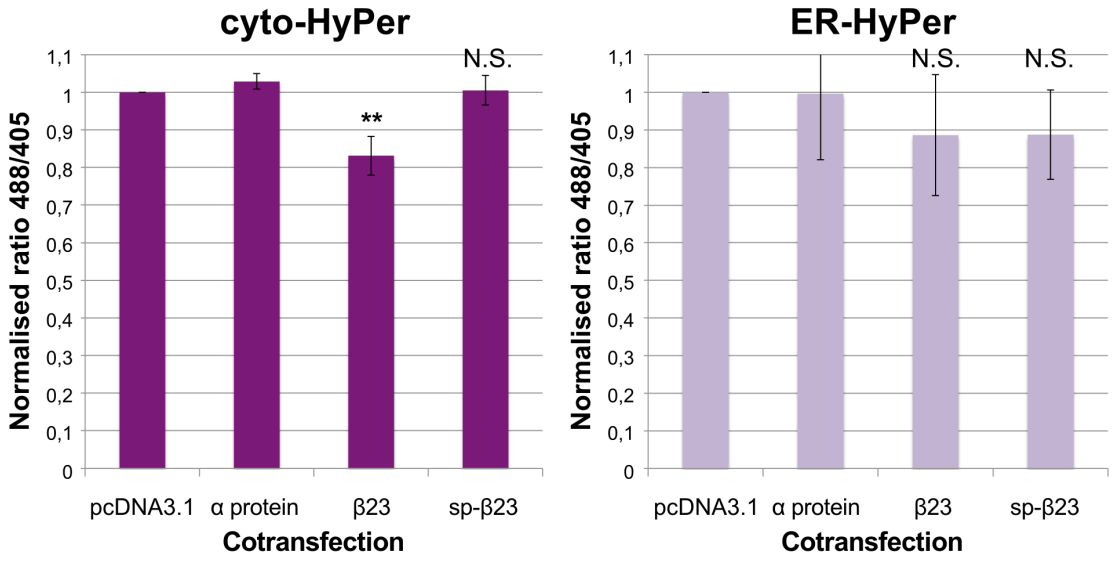

Figure 26: Effects of β23 and sp-β23 on the redox environment in the cytosol (left) and the ER (right) detected with HyPer. For comparison of independent repeats of the experiments the ratios were normalised to the pcDNA3.1 cotransfection. The mean and standard deviation of the normalised ratios are shown for cyto-HyPer (left) and ER-HyPer (right) based on three independent experiments each. The cotransfections with pcDNA3.1 and α protein serve as negative controls. The significance of shifts in the ratios relative to the ratio of the α protein cotransfection is indicated by N.S. (p-value ≥ 0.1), * (p-value < 0.05), ** (p-value < 0.01).

In summary, both β proteins displayed a reducing effect on the redox environment in the ER, detected with both sensors. However, with HyPer the results were not significant, which is probably due to the high variability of ER-HyPer compared to the other sensors (see III.1.3). In contrast, only β23 was found to have a reducing effect in the cytosol and this was only observed using HyPer. The high significance of the HyPer readout together with the high reproducibility of cyto-roGFP suggest that this apparent contradiction regarding the effect of β23 is not a measurement error. If so, the source of the divergent measurements must be the different redox pairs they react to. This would mean that β23 leads to a reduction of the H_2O_2 concentration (which is sensed by HyPer) in the cytosol, but does not influence the GSH/GSSG ratio (sensed by roGFP).

The reducing effect of β23 was also observed with HyPer under highly oxidising and reducing conditions (Figure 27), both in the cytosol and ER. For oxidising conditions the effect was more pronounced, which further strengthens the hypothesis that β23 has a reducing effect.

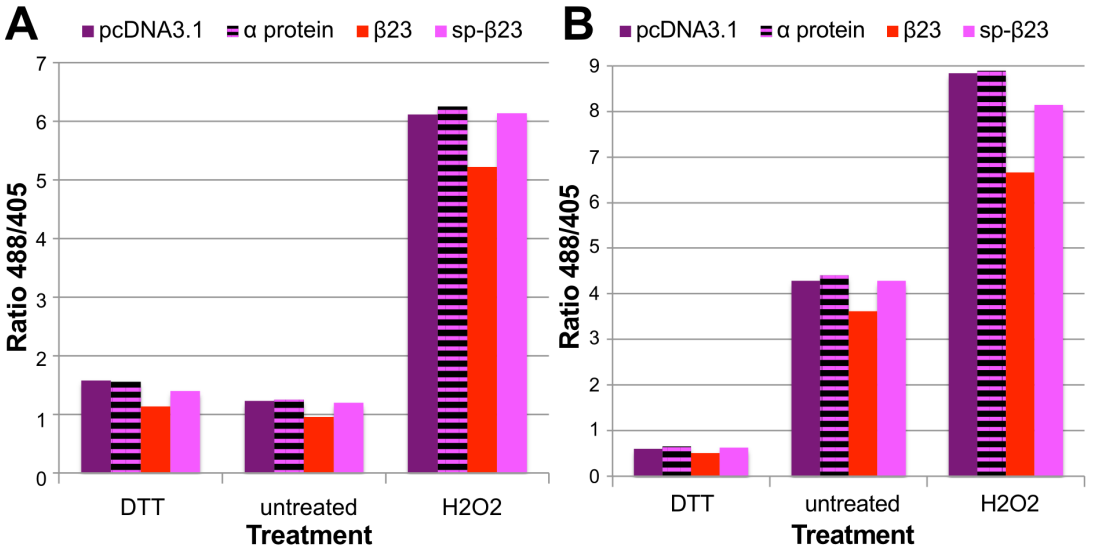

Figure 27: Effects of the redox agents on cells expressing β23 and sp-β23 analysed with cyto-HyPer (A) and ER-HyPer (B). The cotransfections with pcDNA3.1 and α protein serve as negative controls.

2.5. Examining time dependent effects of the β proteins

Next, we were wondering whether the effects of β23 were dependent on the expression time. On the one hand, aggregation is expected to increase over time. On the other hand, cells may adapt to stress caused by the protein aggregates by inducing stress response mechanisms and in this way balance changes in the redox state over time. We thus examined the development of the ratios over time. For this purpose we analysed cells from one transfection cycle after 24 h and 48 h. The cell populations were split 24 h after transfection with a fraction of the cells set apart and collected for a FACS analysis while the rest was cultured for another 24 h.

We compared the effect of the treatments at the two time points to test whether there were differences in the function of the sensor one or two days after transfection (Figure 28). Interestingly, although the ratios upon reduction are equal on both days, we could detect an increase of the ratio upon oxidation at 48 h. This effect was seen for both sensors. ER-roGFP differed comparably in the untreated state. These observations suggest that the sensors gain sensitivity for an oxidising environment with time.

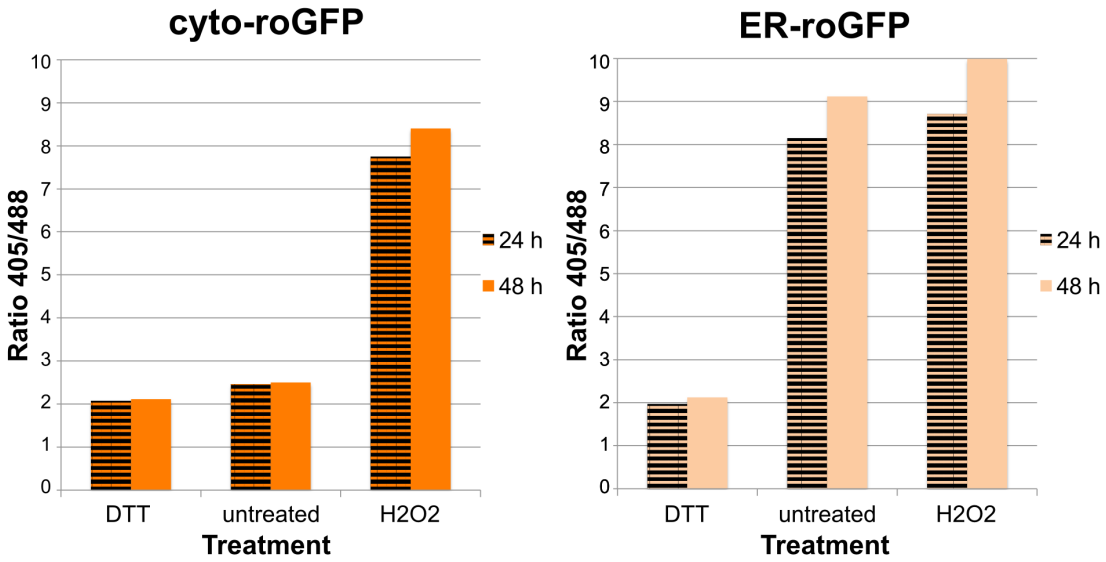

Figure 28: Influence of the time between transfection and measurement on the ratios of roGFP under different redox conditions. Cells from one transfection were harvested after 24 h and after 48 h. The ratios were analysed for cyto-roGFP (left) and ER-roGFP (right).

The same experiment was performed with different cotransfections (Figure 29). This experiment confirms the previous observations, as there is also no difference in the ratios of cytosolic roGFP at the two time points, whereas ER-roGFP again showed increased ratios after 48 h. Most importantly, we could also detect the reducing effect of β23 after 24 h, which once more confirms our findings in this context (see III.2.1).

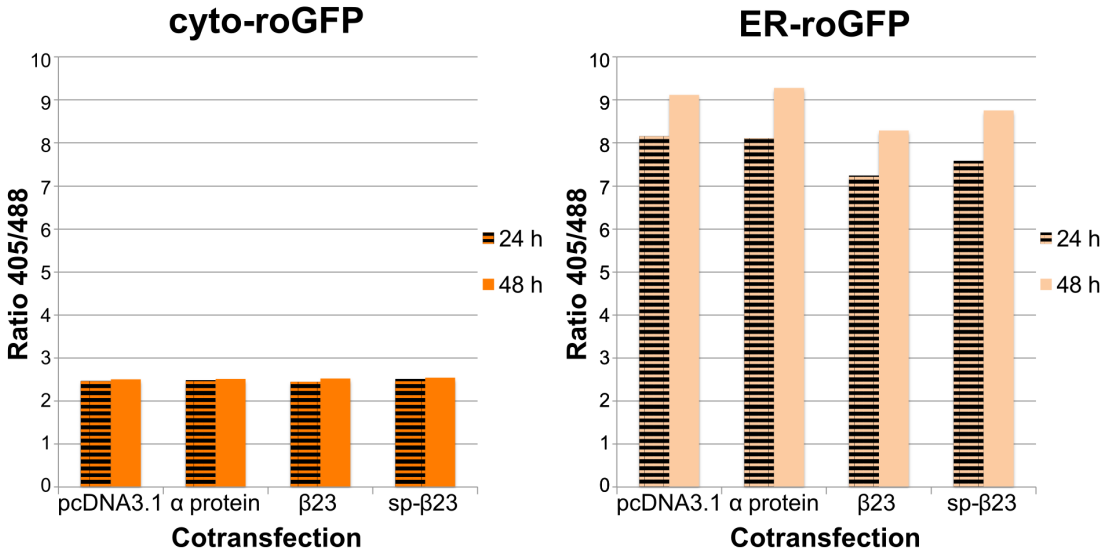

Figure 29: Influence of the time between transfection and measurement on the ratios of roGFP with different cotransfections. Cells from one transfection were harvested after 24 h and after 48 h. The ratios were analysed for cyto-roGFP (left) and ER-roGFP (right).

IV. Conclusion

Beside the successful establishment of experimental methods for measuring redox changes using the redox sensors roGFP and HyPer, each with a cytosolic and an ER-targeted version, this thesis provides insights into the effects of amyloidogenic proteins on the cellular redox environment. The artificial β protein β23, which simulates the protein aggregates that are found in many neurodegenerative diseases, was found to substantially reduce the H_2O_2 concentration but not affect the GSH/GSSG levels in the cytosol. Furthermore, β23 has effects even beyond compartmental boundaries, as we also detected a reducing effect on the redox state (both on the H_2O_2 concentration and on the GSH/GSSG level) of the ER. Interestingly, this cross-compartmental effect was not observed for ER-targeted β23 (sp-β23). We verified the correct localisations of the sensors and the β proteins via immunofluorescence microscopy. Sp-β23 also had a reducing effect on the ER redox state but not on the cytosolic redox state. The reducing effect of sp-β23 was however smaller than the effect of cytosolic β23 on the ER, which could be explained by the fact that the cytosolic variant shows stronger aggregation propensity than sp-β23 as analysed by fluorescence microscopy.

To strengthen these results, we tested the effects of the β23 constructs at two different time points and were able to eliminate a time dependence of the observed reducing effects. In addition, we excluded the possibility of a direct manipulation of the GFP chromophore by the β23 aggregates.

The obtained results are very interesting, yet somewhat surprising. Firstly, the effect of cytosolic β23 aggregates on the ER could be linked to the induction of ER stress, which was found for several cytosolic aggregates of neurodegenerative disease proteins such as the huntingtin protein and α synuclein (Vidal et al., 2011). This connection was suggested based on the increase of ER stress markers upon the expression or the existence of disease proteins. Evidence for a diversity of interferences by the aggregates which all lead to an accumulation of abnormally folded proteins in the ER and thus induce ER stress was found in different studies (Vidal et al., 2011): (i) the blockade of the ER associated protein degradation (ERAD) through the entrapment of essential ERAD proteins; (ii) the impairment of the secretory pathway through the inhibition of vesicle transportation; (iii) an alteration of the protein homeostasis upon occupation of the autophagy system (iv) an interaction with the ER calcium channels leading to perturbations in the calcium homeostasis which is essential for a variety of chaperones and hence influences the correct protein folding in the ER.

However, if the β protein aggregates indeed lead to an induction of ER stress we would have expected a different alteration of the redox state than observed. As described above, ER stress is closely linked to the development of oxidative stress because of the increased H_2O_2 production with the raised demand for protein folding. Thus, we would have expected an increase in the ratios of the redox sensors, but we actually see a reduction in the H_2O_2 level both in the ER and the cytosol. One possible explanation for these unexpected results would be that prolonged ER stress (as it probably is the case after 24-48 h overexpression of aggregating protein) at some point leads

to a breakdown of the oxidases and protein disulphide isomerase and hence a reduction of the H_2O_2 production in the ER. Interestingly, it was previously reported that the knockdown of the major oxidase ERO-1 dramatically shifts the redox state of the ER to reducing conditions (Rual et al., 2004). Since H_2O_2 is an important cellular signalling molecule, a reduction in the ER supply would probably also reduce the amount of H_2O_2 in the cytosol. This finding, together with an overshoot of the detoxifying systems of the cells as a reaction to the primary increase of H_2O_2 after the induction of ER stress and oxidative stress, could explain our observations.

V. Acknowledgements

I am very grateful to Prof. Dr. Franz-Ulrich Hartl for giving me the opportunity to work in his lab for my bachelor's thesis and to Prof. Dr. Michael Groll for the university internal supervision. I would like to thank Lisa Vincenz and Dr. Mark Hipp for their great supervision and support throughout this project. I would further like to thank all other members of the research group that have helped me during the project.

VI. References

Atwood, C.S., Obrenovich, M.E., Liu, T., Chan, H., Perry, G., Smith, M.A., and Martins, R.N. (2003). Amyloid-β: a chameleon walking in two worlds: a review of the trophic and toxic properties of amyloid-β. Brain Res. Rev. *43*, 1–16.

Baruch-Suchodolsky, R., and Fischer, B. (2009). Aβ40, either Soluble or Aggregated, Is a Remarkably Potent Antioxidant in Cell-Free Oxidative Systems. Biochemistry *48*, 4354–4370.

Belousov, V. V, Fradkov, A.F., Lukyanov, K.A., Staroverov, D.B., Shakhbazov, K.S., Terskikh, A. V, and Lukyanov, S. (2006). Genetically encoded fluorescent indicator for intracellular hydrogen peroxide. Nat. Methods *3*, 281–286.

Bence, N.F., Sampat, R.M., and Kopito, R.R. (2001). Impairment of the ubiquitin-proteasome system by protein aggregation. Science *292*, 1552–1555.

Bhandary, B., Marahatta, A., Kim, H.-R., and Chae, H.-J. (2012). An Involvement of Oxidative Stress in Endoplasmic Reticulum Stress and Its Associated Diseases. Int. J. Mol. Sci. *14*, 434–456.

Birk, J., Ramming, T., Odermatt, A., and Appenzeller-Herzog, C. (2013). Green fluorescent protein-based monitoring of endoplasmic reticulum redox poise. Front. Genet. *4*, 1–10.

Campioni, S., Mannini, B., Zampagni, M., Pensalfini, A., Parrini, C., Evangelisti, E., Relini, A., Stefani, M., Dobson, C.M., Cecchi, C., et al. (2010). A causative link between the structure of aberrant protein oligomers and their toxicity. Nat. Chem. Biol. *6*, 140–147.

Chiti, F., and Dobson, C.M. (2006). Protein misfolding, functional amyloid, and human disease. Annu. Rev. Biochem. *75*, 333–366.

Ciryam, P., Tartaglia, G.G., Morimoto, R.I., Dobson, C.M., and Vendruscolo, M. (2013). Widespread aggregation and neurodegenerative diseases are associated with supersaturated proteins. Cell Rep. *5*, 781–790.

Cook, D.G., Forman, M.S., Sung, J.C., Leight, S., Kolson, D.L., Iwatsubo, T., Lee, V.M., and Doms, R.W. (1997). Alzheimer's A beta(1-42) is generated in the endoplasmic reticulum/intermediate compartment of NT2N cells. Nat. Med. *3*, 1021–1023.

Dahlgren, K.N., Manelli, A.M., Stine Jr, W.B., Baker, L.K., Krafft, G.A., and LaDu, M.J. (2002). Oligomeric and fibrillar species of amyloid-β peptides differentially affect neuronal viability. J. Biol. Chem. *277*, 32046–32053.

David, D.C., Ollikainen, N., Trinidad, J.C., Cary, M.P., Burlingame, A.L., and Kenyon, C. (2010). Widespread protein aggregation as an inherent part of aging in C. elegans. PLoS Biol. *8*, 47–48.

Du, H., Guo, L., Yan, S., Sosunov, A.A., McKhann, G.M., and ShiDu Yan, S. (2010). Early deficits in synaptic mitochondria in an Alzheimer's disease mouse model. Proc. Natl. Acad. Sci. *107*, 18670–18675.

Ferreiro, E., Oliveira, C.R., and Pereira, C. (2004). Involvement of endoplasmic reticulum Ca2+ release through ryanodine and inositol 1,4,5-triphosphate receptors in the neurotoxic effects induced by the amyloid-beta peptide. J. Neurosci. Res. *76*, 872–880.

Ferreiro, E., Resende, R., Costa, R., Oliveira, C.R., and Pereira, C.M.F. (2006). An endoplasmic-reticulum-specific apoptotic pathway is involved in prion and amyloid-beta peptides neurotoxicity. Neurobiol. Dis. *23*, 669–678.

Ferreiro, E., Baldeiras, I., Ferreira, I.L., Costa, R.O., Rego, a C., Pereira, C.F., and Oliveira, C.R. (2012). Mitochondrial- and Endoplasmic Reticulum-Associated Oxidative Stress in Alzheimer's Disease: From Pathogenesis to Biomarkers. Int. J. Cell Biol. *2012*, 1–23.

Gella, A., and Durany, N. (2009). Oxidative stress in Alzheimer disease. Cell Adh. Migr. *3*, 88–93.

Gidalevitz, T., Ben-Zvi, A., Ho, K.H., Brignull, H.R., and Morimoto, R.I. (2006). Progressive disruption of cellular protein folding in models of polyglutamine diseases. Science *311*, 1471–1474.

Götz, J., Chen, F., van Dorpe, J., and Nitsch, R.M. (2001). Formation of neurofibrillary tangles in P301l tau transgenic mice induced by Aβ 42 fibrils. Science *293*, 1491–1495.

Gutscher, M., Pauleau, A.-L., Marty, L., Brach, T., Wabnitz, G.H., Samstag, Y., Meyer, A.J., and Dick, T.P. (2008). Real-time imaging of the intracellular glutathione redox potential. Nat. Methods *5*, 553–559.

Hanson, G.T., Aggeler, R., Oglesbee, D., Cannon, M., Capaldi, R.A., Tsien, R.Y., and Remington, S.J. (2004). Investigating mitochondrial redox potential with redox-sensitive green fluorescent protein indicators. J. Biol. Chem. *279*, 13044–13053.

Hartl, F.U., and Hayer-Hartl, M. (2009). Converging concepts of protein folding in vitro and in vivo. Nat. Struct. Mol. Biol. *16*, 574–581.

Hartl, F.U., Bracher, A., and Hayer-Hartl, M. (2011). Molecular chaperones in protein folding and proteostasis. Nature *475*, 324–332.

Hipp, M.S., Park, S.-H., and Hartl, F.U. (2014). Proteostasis impairment in protein-misfolding and -aggregation diseases. Trends Cell Biol.

Hoozemans, J.J.M., van Haastert, E.S., Nijholt, D.A.T., Rozemuller, A.J.M., Eikelenboom, P., and Scheper, W. (2009). The unfolded protein response is activated in pretangle neurons in Alzheimer's disease hippocampus. Am. J. Pathol. *174*, 1241–1251.

Hou, L., and Zagorski, M.G. (2006). NMR Reveals Anomalous Copper(II) Binding to the Amyloid Aβ Peptide of Alzheimer's Disease. J. Am. Chem. Soc. *128*, 9260–9261.

Huang, X., Atwood, C.S., Hartshorn, M.A., Multhaup, G., Goldstein, L.E., Scarpa, R.C., Cuajungco, M.P., Gray, D.N., Lim, J., Moir, R.D., et al. (1999). The Aβ peptide of Alzheimer's disease directly produces hydrogen peroxide through metal ion reduction. Biochemistry *38*, 7609–7616.

Hwang, C., Sinskey, A., and Lodish, H. (1992). Oxidized redox state of glutathione in the endoplasmic reticulum. Science *257*, 1496–1502.

Kim, Y.E., Hipp, M.S., Bracher, A., Hayer-Hartl, M., and Hartl, F.U. (2013). Molecular chaperone functions in protein folding and proteostasis. Annu. Rev. Biochem. *82*, 323–355.

Lashuel, H.A., and Lansbury, P.T. (2006). Are amyloid diseases caused by protein aggregates that mimic bacterial pore-forming toxins? Q. Rev. Biophys. *39*, 167.

Lee, V.M., Goedert, M., and Trojanowski, J.Q. (2001). Neurodegenerative tauopathies. Annu. Rev. Neurosci. *24*, 1121–1159.

Lindsay, J., Laurin, D., Verreault, R., Hébert, R., Helliwell, B., Hill, G.B., and McDowell, I. (2002). Risk factors for Alzheimer's disease: a prospective analysis from the Canadian Study of Health and Aging. Am. J. Epidemiol. *156*, 445–453.

Lovell, M.A., Robertson, J.D., Teesdale, W.J., Campbell, J.L., and Markesbery, W.R. (1998). Copper, iron and zinc in Alzheimer's disease senile plaques. J. Neurol. Sci. *158*, 47–52.

Madeo, J. (2013). The Role of Oxidative Stress in Alzheimer's Disease. J. Alzheimer's Dis. Park. *03*, 1–5.

Malhotra, J.D., and Kaufman, R.J. (2007). Endoplasmic Reticulum Stress and Oxidative Stress: A Vicious Cycle or a Double-Edged Sword? Antioxid. Redox Signal. *9*, 2277–2294.

Malinouski, M., Zhou, Y., Belousov, V. V, Hatfield, D.L., and Gladyshev, V.N. (2011). Hydrogen Peroxide Probes Directed to Different Cellular Compartments. PLoS One *6*, e14564.

Mecocci, P., MacGarvey, U., and Beal, M.F. (1994). Oxidative damage to mitochondrial DNA is increased in Alzheimer's disease. Ann. Neurol. *36*, 747–751.

Meyer, A.J., and Dick, T.P. (2010). Fluorescent protein-based redox probes. Antioxid. Redox Signal. *13*, 621–650.

Meyer, A.J., Brach, T., Marty, L., Kreye, S., Rouhier, N., Jacquot, J.-P., and Hell, R. (2007). Redox-sensitive GFP in Arabidopsis thaliana is a quantitative biosensor for the redox potential of the cellular glutathione redox buffer. Plant J. *52*, 973–986.

Morimoto, R.I. (2008). Proteotoxic stress and inducible chaperone networks in neurodegenerative disease and aging. Genes Dev. *22*, 1427–1438.

Murphy, M. (2009). How mitochondria produce reactive oxygen species. Biochem. J. *417*, 1.

Nowakowski, R.S. (2006). Stable neuron numbers from cradle to grave. Proc. Natl. Acad. Sci. *103*, 12219–12220.

Olzscha, H., Schermann, S.M., Woerner, A.C., Pinkert, S., Hecht, M.H., Tartaglia, G.G., Vendruscolo, M., Hayer-Hartl, M., Hartl, F.U., and Vabulas, R.M. (2011). Amyloid-like Aggregates Sequester Numerous Metastable Proteins with Essential Cellular Functions. Cell *144*, 67–78.

Opazo, C., Huang, X., Cherny, R.A., Moir, R.D., Roher, A.E., White, A.R., Cappai, R., Masters, C.L., Tanzi, R.E., Inestrosa, N.C., et al. (2002). Metalloenzyme-like activity of Alzheimer's disease β-amyloid. Cu-dependent catalytic conversion of dopamine, cholesterol, and biological reducing agents to neurotoxic H2O2. J. Biol. Chem. *277*, 40302–40308.

Park, S.-H., Kukushkin, Y., Gupta, R., Chen, T., Konagai, A., Hipp, M.S., Hayer-Hartl, M., and Hartl, F.U. (2013). PolyQ proteins interfere with nuclear degradation of cytosolic proteins by sequestering the Sis1p chaperone. Cell *154*, 134–145.

Patergnani, S., Suski, J.M., Agnoletto, C., Bononi, A., Bonora, M., De Marchi, E., Giorgi, C., Marchi, S., Missiroli, S., Poletti, F., et al. (2011). Calcium signaling around Mitochondria Associated Membranes (MAMs). Cell Commun. Signal. *9*, 19.

Querfurth, H.W., and LaFerla, F.M. (2010). Alzheimer's Disease. N. Engl. J. Med. *362*, 329–344.

Reddy, P.H., Manczak, M., Mao, P., Calkins, M.J., Reddy, A.P., and Shirendeb, U. (2010). Amyloid-β and mitochondria in aging and Alzheimer's disease: implications for synaptic damage and cognitive decline. J. Alzheimers. Dis. *20 Suppl 2*, S499–512.

Rizzuto, R., Pinton, P., Carrington, W., Fay, F.S., Fogarty, K.E., Lifshitz, L.M., Tuft, R.A., and Pozzan, T. (1998). Close contacts with the endoplasmic reticulum as determinants of mitochondrial Ca2+ responses. Science *280*, 1763–1766.

Ross, C.A., and Poirier, M.A. (2004). Protein aggregation and neurodegenerative disease. Nat. Med. *10*, S10–S17.

Rual, J.-F., Ceron, J., Koreth, J., Hao, T., Nicot, A.-S., Hirozane-Kishikawa, T., Vandenhaute, J., Orkin, S.H., Hill, D.E., van den Heuvel, S., et al. (2004). Toward improving Caenorhabditis elegans phenome mapping with an ORFeome-based RNAi library. Genome Res. *14*, 2162–2168.

Rubinsztein, D.C. (2006). The roles of intracellular protein-degradation pathways in neurodegeneration. Nature *443*, 780–786.

Rui, Y., Tiwari, P., Xie, Z., and Zheng, J.Q. (2006). Acute impairment of mitochondrial trafficking by beta-amyloid peptides in hippocampal neurons. J. Neurosci. *26*, 10480–10487.

Sánchez, I., Mahlke, C., and Yuan, J. (2003). Pivotal role of oligomerization in expanded polyglutamine neurodegenerative disorders. Nature *421*, 373–379.

Saxena, S., and Caroni, P. (2011). Selective Neuronal Vulnerability in Neurodegenerative Diseases: From Stressor Thresholds to Degeneration. Neuron *71*, 35–48.

Schwarzländer, M., Fricker, M.D., Müller, C., Marty, L., Brach, T., Novak, J., Sweetlove, L.J., Hell, R., and Meyer, A.J. (2008). Confocal imaging of glutathione redox potential in living plant cells. J. Microsc. *231*, 299–316.

Selkoe, D.J. (2002). Alzheimer's Disease Is a Synaptic Failure. Science *298*, 789–791.

Sinha, M., Bhowmick, P., Banerjee, A., and Chakrabarti, S. (2013). Antioxidant role of amyloid β protein in cell-free and biological systems: implication for the pathogenesis of Alzheimer disease. Free Radic. Biol. Med. *56*, 184–192.

Tartaglia, G.G., Pawar, A.P., Campioni, S., Dobson, C.M., Chiti, F., and Vendruscolo, M. (2008). Prediction of aggregation-prone regions in structured proteins. J. Mol. Biol. *380*, 425–436.

Taylor, J.P., Hardy, J., and Fischbeck, K.H. (2002). Toxic proteins in neurodegenerative disease. Science *296*, 1991–1995.

Unterberger, U., Höftberger, R., Gelpi, E., Flicker, H., Budka, H., and Voigtländer, T. (2006). Endoplasmic reticulum stress features are prominent in Alzheimer disease but not in prion diseases in vivo. J. Neuropathol. Exp. Neurol. *65*, 348–357.

Vidal, R., Caballero, B., Couve, A., and Hetz, C. (2011). Converging pathways in the occurrence of endoplasmic reticulum (ER) stress in Huntington's disease. Curr. Mol. Med. *11*, 1–12.

Walsh, D.M., and Selkoe, D.J. (2007). A beta oligomers - a decade of discovery. J. Neurochem. *101*, 1172–1184.

Walsh, D.M., Klyubin, I., Fadeeva, J. V, Cullen, W.K., Anwyl, R., Wolfe, M.S., Rowan, M.J., and Selkoe, D.J. (2002). Naturally secreted oligomers of amyloid beta protein potently inhibit hippocampal long-term potentiation in vivo. Nature *416*, 535–539.

Walter, P., and Ron, D. (2011). The Unfolded Protein Response: From Stress Pathway to Homeostatic Regulation. Science *334*, 1081–1086.

Wei, Y., Liu, T., Sazinsky, S.L., Moffet, D.A., Pelczer, I., and Hecht, M.H. (2003). Stably folded de novo proteins from a designed combinatorial library. Protein Sci. *12*, 92–102.

West, M.W., Wang, W., Patterson, J., Mancias, J.D., Beasley, J.R., and Hecht, M.H. (1999). De novo amyloid proteins from designed combinatorial libraries. Proc. Natl. Acad. Sci. U. S. A. *96*, 11211–11216.

Wild-Bode, C., Yamazaki, T., Capell, A., Leimer, U., Steiner, H., Ihara, Y., and Haass, C. (1997). Intracellular generation and accumulation of amyloid β-peptide terminating at amino acid 42. J. Biol. Chem. *272*, 16085–16088.

Wyss-Coray, T. (2006). Inflammation in Alzheimer disease: Driving force, bystander or beneficial response? Nat. Med. *12*, 1005–1015.

Xiong, H., Buckwalter, B.L., Shieh, H.M., and Hecht, M.H. (1995). Periodicity of polar and nonpolar amino acids is the major determinant of secondary structure in self-assembling oligomeric peptides. Proc. Natl. Acad. Sci. U. S. A. *92*, 6349–6353.

Yu, B.P. (1994). Cellular defenses against damage from reactive oxygen species. Physiol. Rev. *74*, 139–162.

Zhang, G., Gurtu, V., and Kain, S.R. (1996). An enhanced green fluorescent protein allows sensitive detection of gene transfer in mammalian cells. Biochem. Biophys. Res. Commun. *227*, 707–711.